

1 **“Let there be Light”: THE EMERGENCE OF STRUCTURE OUT OF THE** 2 **DARK AGES IN THE EARLY UNIVERSE**

3
4 **Abraham Loeb**

5 *Department of Astronomy, Harvard University, 60 Garden St., Cambridge MA, 02138*

6
7 **Keywords:** dark ages, first stars, high-redshift galaxies, reionization, intergalactic medium

8 9 **Contents**

- 10
11 1. Introduction
12 1.1. Observing our past
13 1.2. The expanding universe
14 2. Galaxy Formation
15 2.1. Growth of linear perturbations
16 2.2. Halo properties
17 2.3. Formation of the first stars
18 2.4. Gamma-ray Bursts: probing the first stars one star at a time
19 2.5. Supermassive black holes
20 2.6. The epoch of reionization
21 2.7. Post-reionization suppression of low-mass galaxies
22 3. Probing the Diffuse Intergalactic Hydrogen
23 3.1. Lyman-alpha absorption
24 3.2. 21-cm absorption or emission
25 4. Conclusions

26 27 **Summary**

28
29 Cosmology is by now a mature experimental science. We are privileged to live at a time when the
30 story of genesis (how the Universe started and developed) can be critically explored by direct
31 observations. Looking deep into the Universe through powerful telescopes we can see images of the
32 Universe when it was younger, because of the finite time it takes light to travel to us from distant
33 sources.

34
35 Existing data sets include an image of the Universe when it was 0.4 million years old (in the form of
36 the cosmic microwave background), as well as images of individual galaxies when the Universe
37 was older than a billion years. But there is a serious challenge: in between these two epochs was a
38 period when the Universe was dark, stars had not yet formed, and the cosmic microwave
39 background no longer traced the distribution of matter. And this is precisely the most interesting
40 period, when the primordial soup evolved into the rich zoo of objects we now see.

41
42 The observers are moving ahead along several fronts. The first involves the construction of large
43 infrared telescopes on the ground and in space that will provide us with new photos of the first
44 galaxies. Current plans include ground-based telescopes which are 24-42 meter in diameter, and
45 NASA's successor to the Hubble Space Telescope, called the James Webb Space Telescope. In
46 addition, several observational groups around the globe are constructing radio arrays that will be
47 capable of mapping the three-dimensional distribution of cosmic hydrogen in the infant Universe.
48 These arrays are aiming to detect the long-wavelength (redshifted 21-cm) radio emission from
49 hydrogen atoms. The images from these antenna arrays will reveal how the non-uniform
50 distribution of neutral hydrogen evolved with cosmic time and eventually was extinguished by the
51 ultra-violet radiation from the first galaxies. Theoretical research has focused in recent years on
52 predicting the expected signals for the above instruments and motivating these ambitious

1 observational projects.

2 3 **1. Introduction**

4 5 **1.1. Observing Our Past**

6
7 When we look at our image reflected off a mirror at a distance of 1 meter, we see the way we
8 looked 6.7 nanoseconds ago, the light travel time to the mirror and back. If the mirror is spaced
9 10^{19} cm \approx 3 pc away, we will see the way we looked twenty one years ago. Light propagates at a
10 finite speed, and so by observing distant regions, we are able to see what the Universe looked like in
11 the past, a light travel time ago (Figure 1). The statistical homogeneity of the Universe on large
12 scales guarantees that what we see far away is a fair statistical representation of the conditions that
13 were present in our region of the Universe a long time ago.

14
15 Figure 1. Cosmology is like archeology. The deeper one looks, the older is the layer that is revealed,
16 owing to the finite propagation speed of light

17
18 This fortunate situation makes cosmology an empirical science. We do not need to guess how the
19 Universe evolved. Using telescopes we can simply see how it appeared at earlier cosmic times. In
20 principle, this allows the entire 13.7 billion year cosmic history of our universe to be reconstructed
21 by surveying the galaxies and other sources of light to large distances (Figure 2). Since a greater
22 distance means a fainter flux from a source of a fixed luminosity, the observation of the earliest
23 sources of light requires the development of sensitive instruments and poses challenges to
24 observers.

25
26 Figure 2. Overview of cosmic history, with the age of the universe shown on the top axis and the
27 corresponding redshift on the bottom axis. Yellow represents regions where the hydrogen is
28 ionized, and gray, neutral regions. Stars form in galaxies located within dark matter concentrations
29 whose typical mass grows with time, starting with $\sim 10^5 M_{\odot}$ (red circles) for the host of the first
30 star, rising to $10^7 - 10^9 M_{\odot}$ (blue circles) for the sources of reionization, and reaching
31 $\sim 10^{12} M_{\odot}$ (green circles) for present-day galaxies like our own Milky Way. Astronomers probe
32 the evolution of the cosmic gas using the absorption of background light (dotted lines) by atomic
33 hydrogen along the line of sight. The classical technique uses absorption by the Lyman- α
34 resonance of hydrogen of the light from bright quasars located within massive galaxies, while a new
35 type of astronomical observation will use the 21-cm line of hydrogen with the cosmic microwave
36 background as the background source

37
38 As the universe expands, photon wavelengths get stretched as well. The factor by which the
39 observed wavelength is increased (i.e. shifted towards the red) relative to the emitted one is denoted
40 by $(1+z)$, where z is the cosmological redshift. Astronomers use the known emission patterns of
41 hydrogen and other chemical elements in the spectrum of each galaxy to measure z . This then
42 implies that the universe has expanded by a factor of $(1+z)$ in linear dimension since the galaxy
43 emitted the observed light, and cosmologists can calculate the corresponding distance and cosmic
44 age for the source galaxy. Large telescopes have allowed astronomers to observe faint galaxies that
45 are so far away that we see them more than twelve billion years back in time. Thus, we know
46 directly that galaxies were in existence as early as 850 million years after the Big Bang, at a redshift
47 of $z \sim 6.5$ or higher.

1
2 | We can in principle image the Universe only if it is transparent. Earlier than 400 000 years after
3 the big bang, the cosmic hydrogen was broken into its constituent electrons and protons (i.e.
4 “ionized”) and the Universe was opaque to scattering by the free electrons in the dense plasma.
5 Thus, telescopes cannot be used to electromagnetically image the infant Universe at earlier times
6 | (or redshifts $> 10^3$). The earliest possible image of the Universe was recorded by the COBE and
7 WMAP satellites, which measured the temperature distribution of the cosmic microwave
8 background (CMB) on the sky (Figure 3).

9
10 Figure 3. Images of the Universe shortly after it became transparent, taken by the *COBE* and *WMAP*
11 satellites (see <http://map.gsfc.nasa.gov/> for details). The slight density inhomogeneities in the
12 otherwise uniform Universe imprinted a map of hot and cold spots (shown here as different colors)
13 in the CMB that is observed today. The existence of these anisotropies was predicted three decades
14 before the technology for taking these images became available, in a number of theoretical papers
15 including Sachs & Wolfe (1967), Rees & Sciama (1968), Silk (1968), Sunyaev & Zeldovich (1970),
16 and Peebles & Yu (1970).

17
18 The CMB, the relic radiation from the hot, dense beginning of the universe, is indeed another major
19 probe of observational cosmology. The universe cools as it expands, so it was initially far denser
20 and hotter than it is today. For hundreds of thousands of years the cosmic gas consisted of plasma of
21 free protons and electrons, and a slight mix of light nuclei, sustained by the intense thermal motion
22 of these particles. Just like the plasma in our own Sun, the ancient cosmic plasma emitted and
23 | scattered a strong field of visible and ultraviolet photons. As mentioned above, about 400 000
24 years after the Big Bang the temperature of the universe dipped for the first time below a few
25 thousand degrees Kelvin. The protons and electrons were now moving slowly enough that they
26 could attract each other and form hydrogen atoms, in a process known as cosmic recombination.
27 With the scattering of the energetic photons now much reduced, the photons continued traveling in
28 straight lines, mostly undisturbed except that cosmic expansion has redshifted their wavelength into
29 the microwave regime today. The emission temperature of the observed spectrum of these CMB
30 | photons is the same in all directions to one part in 100 000 (Figure 3), which reveals that
31 conditions were nearly uniform in the early universe.

32
33 It was just before the moment of cosmic recombination (when matter started to dominate in energy
34 density over radiation) that gravity started to amplify the tiny fluctuations in temperature and
35 density observed in the CMB data. Regions that started out slightly denser than average began to
36 contract because the gravitational forces were also slightly stronger than average in these regions.
37 Eventually, after hundreds of millions of years of contraction, the overdense regions stopped
38 expanding, turned around, and eventually collapsed to make bound objects such as galaxies. The
39 gas within these collapsed objects cooled and fragmented into stars. This process, however, would
40 have taken too long to explain the abundance of galaxies today, if it involved only the observed
41 cosmic gas. Instead, gravity is strongly enhanced by the presence of dark matter – an unknown
42 substance that makes up the vast majority (83%) of the cosmic density of matter. The motion of
43 stars and gas around the centers of nearby galaxies indicates that each is surrounded by an extended
44 mass of dark matter, and so dynamically-relaxed dark matter concentrations are generally referred
45 to as “halos”.

46
47 According to the standard cosmological model, the dark matter is cold (abbreviated as CDM), i.e., it
48 behaves as a collection of collisionless particles that started out at matter domination with negligible
49 thermal velocities and have evolved exclusively under gravitational forces. The model explains how
50 both individual galaxies and the large-scale patterns in their distribution originated from the small

1 initial density fluctuations. On the largest scales, observations of the present galaxy distribution
 2 have indeed found the same statistical patterns as seen in the CMB, enhanced as expected by
 3 billions of years of gravitational evolution. On smaller scales, the model describes how regions that
 4 were denser than average collapsed due to their enhanced gravity and eventually formed
 5 gravitationally-bound halos, first on small spatial scales and later on larger ones. In this hierarchical
 6 model of galaxy formation, the small galaxies formed first and then merged or accreted gas to form
 7 larger galaxies. At each snapshot of this cosmic evolution, the abundance of collapsed halos, whose
 8 masses are dominated by dark matter, can be computed from the initial conditions using numerical
 9 simulations. The common understanding of galaxy formation is based on the notion that stars
 10 formed out of the gas that cooled and subsequently condensed to high densities in the cores of some
 11 of these halos.

12
 13 Gravity thus explains how some gas is pulled into the deep potential wells within dark matter halos
 14 and forms the galaxies. One might naively expect that the gas outside halos would remain mostly
 15 undisturbed. However, observations show that it has not remained neutral (i.e., in atomic form) but
 16 was largely ionized by the UV radiation emitted by the galaxies. The diffuse gas pervading the
 17 space outside and between galaxies is referred to as the intergalactic medium (IGM). For the first
 18 hundreds of millions of years after cosmological recombination, the so-called cosmic “dark ages”,
 19 the universe was filled with diffuse atomic hydrogen. As soon as galaxies formed, they started to
 20 ionize diffuse hydrogen in their vicinity. Within less than a billion years, most of the IGM was re-
 21 ionized. We have not yet imaged the cosmic dark ages before the first galaxies had formed. One of
 22 the frontiers in current cosmological studies aims to study the cosmic epoch of reionization and the
 23 first generation of galaxies that triggered it.

24 1.2. The Expanding Universe

25
 26 The modern physical description of the Universe as a whole can be traced back to Einstein, who
 27 assumed for simplicity the so-called “cosmological principle”: that the distribution of matter and
 28 energy is homogeneous and isotropic on the largest scales. Today isotropy is well established for
 29 the distribution of faint radio sources, optically-selected galaxies, the X-ray background, and most
 30 importantly the cosmic microwave background (hereafter, CMB). The constraints on homogeneity
 31 are less strict, but a cosmological model in which the Universe is isotropic but significantly
 32 inhomogeneous in spherical shells around our special location, is also excluded.
 33 In General Relativity, the metric for a space which is spatially homogeneous and isotropic is the
 34 Friedman-Robertson-Walker metric, which can be written in the form
 35

$$36 \quad ds^2 = c^2 dt^2 - a^2(t) \left[\frac{dR^2}{1 - k R^2} + R^2 (d\theta^2 + \sin^2 \theta d\phi^2) \right], \quad (1)$$

37
 38 where c is the speed of light, $a(t)$ is the cosmic scale factor which describes expansion in time t ,
 39 and (R, θ, ϕ) are spherical comoving coordinates. The constant k determines the geometry of the
 40 metric; it is positive in a closed Universe, zero in a flat Universe, and negative in an open Universe.
 41 Observers at rest remain at rest, at fixed (R, θ, ϕ) , with their physical separation increasing with
 42 time in proportion to $a(t)$. A given observer sees a nearby observer at physical distance D
 43 receding at the Hubble velocity $H(t)D$, where the Hubble constant at time t
 44 is $H(t) = da(t)/dt$. Light emitted by a source at time t is observed at $t=0$ with a
 45 redshift $z = 1/a(t) - 1$, where we set $a(t=0) \equiv 1$ for convenience.
 46

1
2 The Einstein field equations of General Relativity yield the Friedman equation

3
4
$$H^2(t) = \frac{8\pi G}{3}\rho - \frac{k}{a^2}, \quad (2)$$

5
6 which relates the expansion of the Universe to its matter-energy content. The constant k
7 determines the geometry of the universe; it is positive in a closed universe, zero in a flat universe,
8 and negative in an open universe. For each component of the energy density ρ , with an equation of
9 state $p = p(\rho)$, the density ρ varies with $a(t)$ according to the thermodynamic relation

10
11
$$d(\rho c^2 R^3) = -pd(R^3). \quad (3)$$

12
13 With the critical density

14
15
$$\rho_C(t) \equiv \frac{3H^2(t)}{8\pi G} \quad (4)$$

16
17 defined as the density needed for $k=0$, we define the ratio of the total density to the critical
18 density as

19
20
$$\Omega \equiv \frac{\rho}{\rho_C}. \quad (5)$$

21
22 With Ω_m , Ω_Λ and Ω_r denoting the present contributions to Ω from matter (including cold dark
23 matter as well as a contribution Ω_b from ordinary matter [“baryons”] made of protons and
24 neutrons), vacuum density (cosmological constant), and radiation, respectively, the Friedman
25 equation becomes

26
27
$$\frac{H(t)}{H_0} = \left[\frac{\Omega_m}{a^3} + \Omega_\Lambda + \frac{\Omega_r}{a^4} + \frac{\Omega_k}{a^2} \right], \quad (6)$$

28
29 where we define H_0 and $\Omega_0 = \Omega_m + \Omega_\Lambda + \Omega_r$ to be the present values of H and Ω ,
30 respectively, and we let

31
32
$$\Omega_k \equiv -\frac{k}{H_0^2} = 1 - \Omega_m. \quad (7)$$

33
34 In the particularly simple Einstein-de Sitter model ($\Omega_m = 1, \Omega_\Lambda = \Omega_r = \Omega_k = 0$), the scale factor
35 varies as $a(t) \propto t^{2/3}$. Even models with non-zero Ω_Λ or Ω_k approach the Einstein-de Sitter
36 scaling-law at high redshift, i.e. when $(1+z) \gg |\Omega_m^{-1} - 1|$ (as long as Ω_r can be neglected). In

1 | this high- z regime the age of the Universe is

$$2 | \quad 3 | \quad t \approx \frac{2}{3H_0\sqrt{\Omega_m}}(1+z)^{-3/2} \approx 10^9 \text{ yr} \left(\frac{1+z}{7} \right)^{-3/2}. \quad (8)$$

4 | Recent observations confine the standard set of cosmological parameters to a relatively narrow
5 | range. In particular, we seem to live in a universe dominated by a cosmological constant (Λ) and
6 | cold dark matter, or in short a Λ CDM cosmology (with Ω_k so small that it is usually assumed to
7 | equal zero) with an approximately scale-invariant primordial power spectrum of density
8 | fluctuations, i.e., $n \approx 1$ where the initial power spectrum is $P(k) = |\delta_{\mathbf{k}}|^2 \propto k^n$ in terms of the
9 | wavenumber k of the Fourier modes $\delta_{\mathbf{k}}$ (see §1 below). Also, the Hubble constant today is written
10 | as $H_0 = 100h \text{ km s}^{-1}\text{Mpc}^{-1}$ in terms of h , and the overall normalization of the power spectrum
11 | is specified in terms of σ_8 , the root-mean-square amplitude of mass fluctuations in spheres of radius
12 | $8h^{-1} \text{ Mpc}$. For example, the best-fit cosmological parameters matching the WMAP data together
13 | with large-scale gravitational lensing observations are $\sigma_8 = 0.826$, $n = 0.953$, $h = 0.687$,
14 | $\Omega_m = 0.299$, $\Omega_\Lambda = 0.701$ and $\Omega_b = 0.0478$.

Comment [R1]: 2.1?

16 | 2. Galaxy Formation

17 | 2.1. Growth of Linear Perturbations

18 | As noted in the Introduction, observations of the CMB show that the universe at cosmic
19 | recombination (redshift $z \sim 10^3$) was remarkably uniform apart from spatial fluctuations in the
20 | energy density and in the gravitational potential of roughly one part in $\sim 10^5$. The primordial
21 | inhomogeneities in the density distribution grew over time and eventually led to the formation of
22 | galaxies as well as galaxy clusters and large-scale structure. In the early stages of this growth, as
23 | long as the density fluctuations on the relevant scales were much smaller than unity, their evolution
24 | can be understood with a linear perturbation analysis.

25 | As before, we distinguish between fixed and comoving coordinates. Using vector notation, the fixed
26 | coordinate \mathbf{r} corresponds to a comoving position $\mathbf{x} = \mathbf{r}/a$. In a homogeneous Universe with
27 | density ρ , we describe the cosmological expansion in terms of an ideal pressureless fluid of
28 | particles each of which is at fixed \mathbf{x} , expanding with the Hubble flow $\mathbf{v} = H(t)\mathbf{r}$ where
29 | $\mathbf{v} = d\mathbf{r}/dt$. Onto this uniform expansion we impose small perturbations, given by a relative
30 | density perturbation

$$31 | \quad 32 | \quad \delta(\mathbf{x}) = \frac{\rho(\mathbf{r})}{\bar{\rho}} - 1, \quad (9)$$

33 | where the mean fluid density is $\bar{\rho}$, with a corresponding peculiar velocity $\mathbf{u} \equiv \mathbf{v} - H\mathbf{r}$. Then the
34 | fluid is described by the continuity and Euler equations in comoving coordinates:

1

$$2 \quad \left| \frac{\partial \delta}{\partial t} + \frac{1}{a} \nabla \cdot [(1 + \delta) \mathbf{u}] = 0 \right. \quad (10)$$

3

$$4 \quad \left| \frac{\partial \mathbf{u}}{\partial t} + H \mathbf{u} + \frac{1}{a} (\mathbf{u} \cdot \nabla) \mathbf{u} = -\frac{1}{a} \nabla \phi. \right. \quad (11)$$

5

6 The potential ϕ is given by the Poisson equation, in terms of the density perturbation:

7

$$8 \quad \left| \nabla^2 \phi = 4\pi G \bar{\rho} a^2 \delta. \right. \quad (12)$$

9

10 This fluid description is valid for describing the evolution of collisionless cold dark matter particles
 11 until different particle streams cross. This “shell-crossing” typically occurs only after perturbations
 12 have grown to become non-linear, and at that point the individual particle trajectories must in
 13 general be followed. Similarly, baryons can be described as a pressureless fluid as long as their
 14 temperature is negligibly small, but non-linear collapse leads to the formation of shocks in the gas.
 15 For small perturbations $\delta \ll 1$, the fluid equations can be linearized and combined to yield

16

$$17 \quad \left| \frac{\partial^2 \delta}{\partial t^2} + 2H \frac{\partial \delta}{\partial t} = 4\pi G \bar{\rho} \delta. \right. \quad (13)$$

18

19 This linear equation has in general two independent solutions, only one of which grows with time.
 20 Starting with random initial conditions, this “growing mode” comes to dominate the density
 21 evolution. Thus, until it becomes non-linear, the density perturbation maintains its shape in
 22 comoving coordinates and grows in proportion to a growth factor $D(t)$. The growth factor in the
 23 matter-dominated era is given by

24

$$25 \quad \left| D(t) \propto \frac{(\Omega_\Lambda a^3 + \Omega_k a + \Omega_m)^{1/2}}{a^{3/2}} \int_0^a \frac{a'^{3/2} da'}{(\Omega_\Lambda a'^3 + \Omega_k a' + \Omega_m)^{3/2}}, \right. \quad (14)$$

26

27 where we neglect Ω_r when considering halos forming in the matter-dominated regime at
 28 $z \ll 10^4$. In the Einstein-de Sitter model (or, at high redshift, in other models as well) the growth
 29 factor is simply proportional to $a(t)$.

30

31 The spatial form of the initial density fluctuations can be described in Fourier space, in terms of
 32 Fourier components

33

$$34 \quad \left| \delta_{\mathbf{k}} = \int d^3 x \delta(x) e^{-i\mathbf{k} \cdot \mathbf{x}}. \right. \quad (15)$$

35

36 Here we use the comoving wave-vector \mathbf{k} , whose magnitude k is the comoving wavenumber
 37 which is equal to 2π divided by the wavelength. The Fourier description is particularly simple for
 38 fluctuations generated by inflation. Inflation generates perturbations given by a Gaussian random

field, in which different \mathbf{k} -modes are statistically independent, each with a random phase. The statistical properties of the fluctuations are determined by the variance of the different \mathbf{k} -modes and the variance is described in terms of the power spectrum $P(k)$ as follows:

$$\langle \delta_{\mathbf{k}} \delta_{\mathbf{k}'}^* \rangle = (2\pi)^3 P(k) \delta^{(3)}(\mathbf{k} - \mathbf{k}'), \quad (16)$$

where $\delta^{(3)}$ is the three-dimensional Dirac delta function. The gravitational potential fluctuations are sourced by the density fluctuations through Poisson's equation.

In standard models, inflation produces a primordial power-law spectrum $P(k) \propto k^n$ with $n \sim 1$. Perturbation growth in the radiation-dominated and then matter-dominated Universe results in a modified final power spectrum, characterized by a turnover at a scale of order the horizon cH^{-1} at matter-radiation equality, and a small-scale asymptotic shape of $P(k) \propto k^{n-4}$. The overall amplitude of the power spectrum is not specified by current models of inflation, and it is usually set by comparing to the observed CMB temperature fluctuations or to local measures of large-scale structure.

Since density fluctuations may exist on all scales, in order to determine the formation of objects of a given size or mass it is useful to consider the statistical distribution of the smoothed density field.

Using a window function $W(\mathbf{r})$ normalized so that $\int d^3r W(\mathbf{r}) = 1$, the smoothed density perturbation field, $\int d^3r \delta(\mathbf{x}) W(\mathbf{r})$, itself follows a Gaussian distribution with zero mean. For the particular choice of a spherical top-hat, in which $W = 1$ in a sphere of radius R and is zero outside, the smoothed perturbation field measures the fluctuations in the mass in spheres of radius R . The normalization of the present power spectrum is often specified by the value of $\sigma_8 \equiv \sigma(R = 8h^{-1}\text{Mpc})$. For the top-hat, the smoothed perturbation field is denoted δ_R or δ_M , where the mass M is related to the comoving radius R by $M = 4\pi\rho_m R^3 / 3$, in terms of the current mean density of matter ρ_m . The variance $\langle \delta_M \rangle^2$ is

$$\sigma^2(M) = \sigma^2(R) = \int_0^\infty \frac{dk}{2\pi^2} k^2 P(k) \left[\frac{3j_1(kR)}{kR} \right]^2, \quad (17)$$

where $j_1(x) = (\sin x - x \cos x) / x^2$. The function $\sigma(M)$ plays a crucial role in estimates of the abundance of collapsed objects, as we describe later.

Different physical processes contributed to the perturbation growth. In the absence of other influences, gravitational forces due to density perturbations imprinted by inflation would have driven parallel perturbation growth in the dark matter, baryons and photons. However, since the photon sound speed is of order the speed of light, the radiation pressure produced sound waves on a scale of order the cosmic horizon and suppressed sub-horizon perturbations in the photon density. The baryonic pressure similarly suppressed perturbations in the gas below the (much smaller) so-

1 called baryonic *Jeans* scale. Since the formation of hydrogen at recombination had decoupled the
2 cosmic gas from its mechanical drag on the CMB, the baryons subsequently began to fall into the
3 pre-existing gravitational potential wells of the dark matter.

4
5 Spatial fluctuations developed in the gas temperature as well as in the gas density. Both the baryons
6 and the dark matter were affected on small scales by the temperature fluctuations through the gas
7 pressure. Compton heating due to scattering of the residual free electrons (constituting a fraction
8 $\sim 10^{-4}$) with the CMB photons remained effective, keeping the gas temperature fluctuations tied to
9 the photon temperature fluctuations, even for a time after recombination. The growth of linear
10 perturbations can be calculated with the standard CMBFAST code (<http://www.cmbfast.org>), after a
11 modification to account for the fact that the speed of sound of the gas also fluctuates spatially.

12
13 Figure 4. Power spectra of density and temperature fluctuations vs. comoving wavenumber, at
14 redshifts 1200, 800, 400, and 200 (from Barkana & Loeb 2007). We consider fluctuations in the
15 CDM density (solid curves), baryon density (dotted curves), baryon temperature (short-dashed
16 curves), and photon temperature (long-dashed curves).

17
18 The magnitude of the fluctuations in the CDM and baryon densities, and in the baryon and photon
19 temperatures, is shown in Figure 4, in terms of the dimensionless combination
20 $[k^3 P(k) / (2\pi^2)]^{1/2}$, where $P(k)$ is the corresponding power spectrum of fluctuations in terms
21 of the comoving wavenumber k of each Fourier mode. After recombination, two main drivers
22 affect the baryon density and temperature fluctuations, namely, the thermalization with the CMB
23 and the gravitational force that attracts the baryons to the dark matter potential wells. As shown in
24 the figure, the density perturbations in all species grow together on scales where gravity is
25 unopposed, outside the horizon (i.e., at $k < 0.01 \text{ Mpc}^{-1}$ at $z \sim 1000$). At $z = 1200$ the
26 perturbations in the baryon-photon fluid oscillate as acoustic waves on scales of order the sound
27 horizon ($k \sim 0.01 \text{ Mpc}^{-1}$), while smaller-scale perturbations in both the photons and baryons are
28 damped by photon diffusion and the drag of the diffusing photons on the baryons. On sufficiently
29 small scales the power spectra of baryon density and temperature roughly assume the shape of the
30 dark matter fluctuations (except for the gas-pressure cutoff at the very smallest scales), due to the
31 effect of gravitational attraction on the baryon density and of the resulting adiabatic expansion on
32 the gas temperature. After the mechanical coupling of the baryons to the photons ends at $z \sim 1000$,
33 the baryon density perturbations gradually grow towards the dark matter perturbations because of
34 gravity. Similarly, after the thermal coupling ends at $z \sim 200$, the baryon temperature fluctuations
35 are driven by adiabatic expansion towards a value of 2/3 of the density fluctuations. As the figure
36 shows, by $z = 200$ the baryon infall into the dark matter potentials is well advanced and adiabatic
37 expansion is becoming increasingly important in setting the baryon temperature.

38 39 2.2. Halo Properties

40
41 The small density fluctuations evidenced in the CMB grow over time as described in the previous
42 subsection, until the perturbation δ becomes of order unity, and the full non-linear gravitational
43 problem must be considered. The dynamical collapse of a dark matter halo can be solved
44 analytically only in cases of particular symmetry. If we consider a region which is much smaller
45 than the horizon cH^{-1} , then the formation of a halo can be formulated as a problem in Newtonian
46 gravity, in some cases with minor corrections coming from General Relativity. The simplest case is
47 that of spherical symmetry, with an initial ($t = t_i \ll t_0$) top-hat of uniform overdensity δ_1 inside a

1 | sphere of radius R . Although this model is restricted in its direct applicability, the results of
2 | spherical collapse have turned out to be surprisingly useful in understanding the properties and
3 | distribution of halos in models based on cold dark matter.

4 |
5 | The collapse of a spherical top-hat perturbation is described by the Newtonian equation (with a
6 | correction for the cosmological constant)

$$7 | \frac{d^2 r}{dt^2} = H_0^2 \Omega_\Lambda r - \frac{GM}{r^2}, \quad (18)$$

9 |
10 | where r is the radius in a fixed (not comoving) coordinate frame, H_0 is the present-day Hubble
11 | constant, M is the total mass enclosed within radius r , and the initial velocity field is given by the
12 | Hubble flow $dr/dt = H(t)r$. The enclosed δ grows initially as $\delta_L = \delta_1 D(t)/D(t_1)$, in
13 | accordance with linear theory, but eventually δ grows above δ_L . If the mass shell at radius r is
14 | bound (i.e., if its total Newtonian energy is negative) then it reaches a radius of maximum
15 | expansion and subsequently collapses. As demonstrated in the previous section, at the moment
16 | when the top-hat collapses to a point, the overdensity predicted by linear theory is $\delta_L = 1.686$ in
17 | the Einstein-de Sitter model, with only a weak dependence on Ω_m and Ω_Λ . Thus a tophat
18 | collapses at redshift z if its linear overdensity extrapolated to the present day (also termed the
19 | critical density of collapse) is

$$21 | \delta_{\text{crit}}(z) = \frac{1.686}{D(z)}, \quad (19)$$

22 |
23 | where we set $D(z=0) = 1$.

24 |
25 | Even a slight violation of the exact symmetry of the initial perturbation can prevent the tophat from
26 | collapsing to a point. Instead, the halo reaches a state of virial equilibrium by violent relaxation
27 | (phase mixing). Using the virial theorem $U = -2K$ to relate the potential energy U to the kinetic
28 | energy K in the final state (implying that the virial radius is half the turnaround radius - where the
29 | kinetic energy vanishes), the final overdensity relative to the critical density at the collapse redshift
30 | is $\Delta_c = 18\pi^2 \approx 178$ in the Einstein-de Sitter model, modified in a Universe with $\Omega_m + \Omega_\Lambda = 1$
31 | to the fitting formula

$$33 | \Delta_c = 18\pi^2 + 82d - 39d^2, \quad (20)$$

34 |
35 | where $d \equiv \Omega_m^z - 1$ is evaluated at the collapse redshift, so that

$$37 | \Omega_m^z = \frac{\Omega_m (1+z)^3}{\Omega_m (1+z)^3 + \Omega_\Lambda + \Omega_k (1+z)^2}. \quad (21)$$

38 |
39 | A halo of mass M collapsing at redshift z thus has a virial radius

Deleted: .

$$r_{\text{vir}} = 0.784 \left(\frac{M}{10^8 h^{-1} M_{\odot}} \right)^{1/3} \left[\frac{\Omega_m \Delta_c}{\Omega_m^z 18\pi^2} \right]^{-1/3} \left(\frac{1+z}{10} \right)^{-1} h^{-1} \text{kpc}, \quad (22)$$

and a corresponding circular velocity,

$$V_c = \left(\frac{GM}{r_{\text{vir}}} \right)^{1/2} = 23.4 \left(\frac{M}{10^8 h^{-1} M_{\odot}} \right)^{1/3} \left[\frac{\Omega_m \Delta_c}{\Omega_m^z 18\pi^2} \right]^{1/6} \left(\frac{1+z}{10} \right)^{1/2} \text{kms}^{-1}. \quad (23)$$

Deleted: .

In these expressions we have assumed a present Hubble constant written in the form $H_0 = 100 h \text{ km s}^{-1} \text{ Mpc}^{-1}$. We may also define a virial temperature

$$T_{\text{vir}} = \frac{\mu m_p V_c^2}{2k} = 1.98 \times 10^4 \left(\frac{\mu}{0.6} \right) \left(\frac{M}{10^8 h^{-1} M_{\odot}} \right)^{2/3} \left[\frac{\Omega_m \Delta_c}{\Omega_m^z 18\pi^2} \right]^{1/3} \left(\frac{1+z}{10} \right) \text{K}, \quad (24)$$

where μ is the mean molecular weight and m_p is the proton mass. Note that the value of μ depends on the ionization fraction of the gas; for a fully ionized primordial gas $\mu = 0.59$, while a gas with ionized hydrogen but only singly-ionized helium has $\mu = 0.61$. The binding energy of the halo is approximately,

$$E_b = \frac{1}{2} \frac{GM^2}{r_{\text{vir}}} = 5.45 \times 10^{53} \left(\frac{M}{10^8 h^{-1} M_{\odot}} \right)^{5/3} \left[\frac{\Omega_m \Delta_c}{\Omega_m^z 18\pi^2} \right]^{1/3} \left(\frac{1+z}{10} \right) h^{-1} \text{erg}. \quad (25)$$

(The coefficient of $1/2$ in equation (25) would be exact for a singular isothermal sphere with $\rho(r) \propto 1/r^2$.)

Note that the binding energy of the baryons is smaller by a factor equal to the baryon fraction Ω_b / Ω_m .

Although spherical collapse captures some of the physics governing the formation of halos, structure formation in cold dark matter models proceeds hierarchically. At early times, most of the dark matter is in low-mass halos, and these halos continuously accrete and merge to form high-mass halos. Numerical simulations of hierarchical halo formation indicate a roughly universal spherically-averaged density profile for the resulting halos, though with considerable scatter among different halos. The typical profile has the form

$$\rho(r) = \frac{3H_0^2}{8\pi G} (1+z)^3 \frac{\Omega_m}{\Omega_m^z} \frac{\delta_c}{c_N x (1+c_N x)^2}, \quad (26)$$

1 | where $x = r / r_{\text{vir}}$, and the characteristic density δ_c is related to the concentration parameter c_N
2 | by

$$\delta_c = \frac{\Delta_c}{3} \frac{c_N^3}{\ln(1 + c_N) - c_N / (1 + c_N)}. \quad (27)$$

5 |
6 | The concentration parameter itself depends on the halo mass M , at a given redshift z .

7 | 2.3. Formation of the First Stars

8 |
9 |
10 | Theoretical expectations for the properties of the first galaxies are based on the standard
11 | cosmological model outlined in the Introduction. The formation of the first bound objects marked
12 | the central milestone in the transition from the initial simplicity (discussed in the previous
13 | subsection) to the present-day complexity. Stars and accreting black holes output copious radiation
14 | and also produced explosions and outflows that brought into the IGM chemical products from
15 | stellar nucleosynthesis and enhanced magnetic fields. However, the formation of the very first stars,
16 | in a universe that had not yet suffered such feedback, remains a well-specified problem for
17 | theorists.

18 |
19 | Figure 5. Collapse and fragmentation of a primordial cloud of gas (from Bromm & Loeb 2004).

20 | Shown is the projected gas density at a redshift $z \simeq 21.5$, briefly after gravitational runaway
21 | collapse has commenced in the center of the cloud. The refined morphology is plotted in a
22 | simulation box with linear physical size of 0.5 pc. The central density peak, vigorously gaining
23 | mass by accretion, defines the seed of a metal-free (Population III) star. Searches for metal-poor
24 | stars are underway in the halo of the Milky Way galaxy, an environment less crowded by metal-rich
25 | (Population I,II) stars than the core of our galaxy. The goal of these searches is to constrain
26 | theoretical calculations (such as the one shown here) for the formation of the first stars.

27 |
28 | Stars form when huge amounts of matter collapse to enormous densities. However, the process can
29 | be stopped if the pressure exerted by the hot intergalactic gas prevents outlying gas from falling into
30 | dark matter concentrations. As the gas falls into a dark matter halo, it forms shocks due to
31 | converging supersonic flows and in the process heats up and can only collapse further by first
32 | radiating its energy away. This restricts this process of collapse to very large clumps of dark matter
33 | that are around 100000 times the mass of the Sun. Inside these clumps, the shocked gas loses
34 | energy by emitting radiation from excited molecular hydrogen that formed naturally within the
35 | primordial gas mixture of hydrogen and helium.

36 |
37 | The first stars are expected to have been quite different from the stars that form today in the Milky
38 | Way. The higher pressure within the primordial gas due to the presence of fewer cooling agents
39 | suggests that fragmentation only occurred into relatively large units, in which gravity could
40 | overcome the pressure. Due to the lack of carbon, nitrogen, and oxygen – elements that would
41 | normally dominate the nuclear energy production in modern massive stars – the first stars must
42 | have condensed to extremely high densities and temperatures before nuclear reactions were able to
43 | heat the gas and balance gravity. These unusually massive stars produced high luminosities of UV
44 | photons, but their nuclear fuel was exhausted after 2–3 million years, resulting in a huge supernova
45 | or in collapse to a black hole. The heavy elements which were dispersed by the first supernovae in
46 | the surrounding gas, enabled the enriched gas to cool more effectively and fragment into lower
47 | mass stars. Simple calculations indicate that a carbon or oxygen enrichment of merely $< 10^{-3}$ of
48 | the solar abundance is sufficient to allow solar mass stars to form. These second-generation “low-

1 metallicity” stars are long-lived and could in principle be discovered in the halo of the Milky Way
2 galaxy, providing fossil record of the earliest star formation episode in our cosmic environment.

3
4 Advances in computing power have made possible detailed numerical simulations of how the first
5 stars formed. These simulations begin in the early universe, in which dark matter and gas are
6 distributed uniformly, apart from tiny variations in density and temperature that are statistically
7 distributed according to the patterns observed in the CMB. In order to span the vast range of scales
8 needed to simulate an individual star within a cosmological context, the latest code follows a box
9 0.3 Mpc in length and zooms in repeatedly on the densest part of the first collapsing cloud that is
10 found within the simulated volume. The simulation follows gravity, hydrodynamics, and chemical
11 processes in the primordial gas, and resolves to a scale which is 10 orders smaller in magnitude than
12 that of the simulated box. While the resolved scale is still three orders of magnitudes larger than the
13 size of the Sun, these simulations have established that the first stars formed within halos containing
14 $\sim 10^5 M_{\odot}$ in total mass, and indicate that the first stars most likely weighed $\sim 100 M_{\odot}$ each.

15
16 To estimate *when* the first stars formed we must remember that the first $100\,000$ solar mass halos
17 collapsed in regions that happened to have a particularly high density enhancement very early on.
18 There was initially only a small abundance of such regions in the entire universe, so a simulation
19 that is limited to a small volume is unlikely to find such halos until much later. Simulating the entire
20 universe is well beyond the capabilities of current simulations, but analytical models predict that the
21 first observable star in the universe probably formed 30 million years after the Big Bang, less than a
22 quarter of one percent of the Universe’s total age of 13.7 billion years.

23
24 Although stars were extremely rare at first, gravitational collapse increased the abundance of
25 galactic halos and star formation sites with time (Figure 2). Radiation from the first stars is expected
26 to have eventually dissociated all the molecular hydrogen in the intergalactic medium, leading to
27 the domination of a second generation of larger galaxies where the gas cooled via radiative
28 transitions in atomic hydrogen and helium. Atomic cooling occurred in halos of mass above
29 $\sim 10^8 M_{\odot}$, in which the infalling gas was heated above 10,000 K and became ionized. The first
30 galaxies to form through atomic cooling are expected to have formed around redshift 45, and such
31 galaxies were likely the main sites of star formation by the time reionization began in earnest. As
32 the IGM was heated above 10,000 K by reionization, its pressure jumped and prevented the gas
33 from accreting into newly forming halos below $\sim 10^9 M_{\odot}$. The first Milky-Way-sized halo
34 $M = 10^{12} M_{\odot}$ is predicted to have formed 400 million years after the Big Bang, but such halos
35 have become typical galactic hosts only in the last five billion years.

36
37 Hydrogen is the most abundant element in the Universe, The prominent Lyman- α spectral line of
38 hydrogen (corresponding to a transition from its first excited level to its ground state) provides an
39 important probe of the condensation of primordial gas into the first galaxies. Existing searches for
40 Lyman- α emission have discovered galaxies robustly out to a redshift $z \sim 7$ with some
41 unconfirmed candidate galaxies out to $z \sim 10$. The spectral break owing to Lyman- α absorption
42 by the IGM allows identifying high-redshifts galaxies photometrically. Existing observations
43 provide only a preliminary glimpse into the formation of the first galaxies.

44
45 Within the next decade, NASA plans to launch an infrared space telescope (*JWST*; Figure 6) that
46 will image some of the earliest sources of light (stars and black holes) in the Universe. In parallel,
47 there are several initiatives to construct large-aperture infrared telescopes on the ground with the
48 same goal in mind (see <http://www.eso.org/public/astronomy/projects/e-elt.html>;

1 <http://www.tmt.org/>; <http://www.gmto.org/>).

2
3 Figure 6. A sketch of the current design for the *James Webb Space Telescope*, the successor to the
4 *Hubble Space Telescope* to be launched in 2013 (see <http://www.jwst.nasa.gov/>). The current design
5 includes a primary mirror made of beryllium which is 6.5 meters in diameter as well as an
6 instrument sensitivity that spans the full range of infrared wavelengths of 0.6–28 μm and will allow
7 detection of some of the first galaxies in the infant Universe. The telescope will orbit 1.5 million km
8 from Earth at the Lagrange L2 point. Note that the sun shield (the large flat screen in the image) is
9 $22\text{m} \times 10\text{m}$ in size.

10
11 The next generation of ground-based telescopes will have a diameter of twenty to thirty meters
12 (Figure 7). Together with *JWST* (which will not be affected by the atmospheric background) they
13 will be able to image and make spectral studies of the early galaxies. Given that these galaxies also
14 create the ionized bubbles around them by their UV emission, during reionization the locations of
15 galaxies should correlate with bubbles within the neutral hydrogen. Within a decade it should be
16 possible to explore the environmental influence of individual galaxies by using these telescopes in
17 combination with 21-cm probes of reionization.

18
19 Figure 7. Artist's conception of the design for one of the future giant telescopes that might detect
20 the first generation of galaxies from the ground. The *Giant Magellan Telescope (GMT)* is designed
21 to contain seven mirrors (each 8.4 meter in diameter) and to have a resolving power equivalent to a
22 24.5 meter (80 foot) primary mirror. For more details see <http://www.gmto.org/>. Two other teams
23 are designing competing large telescopes, namely the *Thirty Meter Telescope* (see
24 <http://www.tmt.org/>) and the *European Extremely Large Telescope* (see <http://www.eso.org/public/astronomy/projects/e-elt.html>).

25 26 27 **2.4. Gamma-Ray Bursts: Probing the First Stars One Star at a Time**

28
29 So far, to learn about diffuse IGM gas pervading the space outside and between galaxies,
30 astronomers routinely study its absorption signatures in the spectra of distant quasars, the brightest
31 long-lived astronomical objects. Quasars' great luminosities are believed to be powered by
32 accretion of gas onto black holes weighing up to a few billion times the mass of the Sun that are
33 situated in the centers of massive galaxies. As the surrounding gas spirals in toward the black hole
34 sink, the viscous dissipation of heat makes the gas glow brightly into space, creating a luminous
35 source visible from afar.

36
37 Over the past decade, an alternative population of bright sources at cosmological distances was
38 discovered, the so-called afterglows of *Gamma-Ray Bursts (GRBs)*. These events are characterized
39 by a flash of high-energy (> 0.1 MeV) photons, typically lasting 0.1–100 seconds, which is
40 followed by an afterglow of lower-energy photons over much longer timescales. The afterglow
41 peaks at X-ray, UV, optical and eventually radio wavelengths on time scales of minutes, hours,
42 days, and months, respectively. The central engines of GRBs are believed to be associated with the
43 compact remnants (neutron stars or stellar-mass black holes) of massive stars. Their high
44 luminosities make them detectable out to the edge of the visible Universe. GRBs offer the
45 opportunity to detect the most distant (and hence earliest) population of massive stars, the so-called
46 Population III (or Pop III), one star at a time (Figure 8). In the hierarchical assembly process of
47 halos that are dominated by cold dark matter (CDM), the first galaxies should have had lower
48 masses (and lower stellar luminosities) than their more recent counterparts. Consequently, the
49 characteristic luminosity of galaxies or quasars is expected to decline with increasing redshift. GRB
50 afterglows, which already produce a peak flux comparable to that of quasars or starburst galaxies at
51 $z \sim 1-2$, are therefore expected to outshine any competing source at the highest redshifts, when

1 the first dwarf galaxies formed in the Universe.

2
3 Figure 8. Illustration of a long-duration gamma-ray burst in the popular “collapsar” model. The
4 collapse of the core of a massive star (which lost its hydrogen envelope) to a black hole generates
5 two opposite jets moving out at a speed close to the speed of light. The jets drill a hole in the star
6 and shine brightly towards an observer who happens to be located within with the collimation cones
7 of the jets. The jets emanating from a single massive star are so bright that they can be seen across
8 the Universe out to the epoch when the first stars formed (for more information see
9 <http://swift.gsfc.nasa.gov/>).

10
11 GRBs, the electromagnetically-brightest explosions in the Universe, should be detectable out to
12 redshifts $z > 10$. High-redshift GRBs can be identified through infrared photometry, based on the
13 Lyman- α break induced by absorption of their spectrum at wavelengths below
14 $1.216 \mu\text{m}[(1+z)/10]$. Follow-up spectroscopy of high-redshift candidates can then be
15 performed on a 10-meter-class telescope. GRB afterglows offer the opportunity to detect stars as
16 well as to probe the metal enrichment level of the intervening IGM. Recently, the *Swift* satellite has
17 detected a GRB originating at $z \approx 6.3$, thus demonstrating the viability of GRBs as probes of the
18 early Universe.

19
20 Another advantage of GRBs is that the GRB afterglow flux at a given observed time lag after the
21 γ -ray trigger is not expected to fade significantly with increasing redshift, since higher redshifts
22 translate to earlier times in the source frame, during which the afterglow is intrinsically brighter.
23 For standard afterglow lightcurves and spectra, the increase in the luminosity distance with redshift
24 is compensated by this *cosmological time-stretching* effect as shown in Figure 9.

25
26 Figure 9. GRB afterglow flux as a function of time since the γ -ray trigger in the observer frame
27 (from Barkana & Loeb 2004a). The flux (solid curves) is calculated at the redshifted Lyman- α
28 wavelength. The dotted curves show the planned detection threshold for the *James Webb Space*
29 *Telescope (JWST)*, assuming a spectral resolution $R = 5000$ with the near infrared spectrometer, a
30 signal to noise ratio of 5 per spectral resolution element, and an exposure time equal to 20% of the
31 time since the GRB explosion (see <http://www.ngst.stsci.edu/nms/main/>). Each set of curves shows
32 a sequence of redshifts, namely $z = 5, 7, 9, 11, 13, \text{ and } 15$, respectively, from top to bottom.

33
34 GRB afterglows have smooth (broken power-law) continuum spectra unlike quasars which show
35 strong spectral features (such as broad emission lines or the so-called “blue bump”) that complicate
36 the extraction of IGM absorption features. In particular, the extrapolation into the spectral regime
37 marked by the IGM Lyman- α absorption during the epoch of reionization is much more
38 straightforward for the smooth UV spectra of GRB afterglows than for quasars with an underlying
39 broad Lyman- α emission line. However, the interpretation may be complicated by the presence of
40 damped Lyman- α absorption by dense neutral hydrogen in the immediate environment of the GRB
41 within its host galaxy. Since GRBs originate from the dense environment of active star formation,
42 such damped absorption is expected and indeed has been seen, including in the most distant GRB at
43 $z = 6.3$.

44 2.5. Supermassive Black Holes

45
46 The fossil record in the present-day Universe indicates that every bulged galaxy hosts a
47 supermassive black hole (BH) at its center. This conclusion is derived from a variety of techniques
48

1 which probe the dynamics of stars and gas in galactic nuclei. The inferred BHs are dormant or faint
2 most of the time, but occasionally flash in a short burst of radiation that lasts for a small fraction of
3 the age of the Universe. The short duty cycle accounts for the fact that bright quasars are much less
4 abundant than their host galaxies, but it begs the more fundamental question: *why is the quasar*
5 *activity so brief?* A natural explanation is that quasars are suicidal, namely the energy output from
6 the BHs regulates their own growth.

7
8 Supermassive BHs make up a small fraction, $< 10^{-3}$, of the total mass in their host galaxies, and so
9 their direct dynamical impact is limited to the central star distribution where their gravitational
10 influence dominates. Dynamical friction on the background stars keeps the BH close to the center.
11 Random fluctuations in the distribution of stars induces a Brownian motion of the BH. This motion
12 can be described by the same Langevin equation that captures the motion of a massive dust particle
13 as it responds to random kicks from the much lighter molecules of air around it. The characteristic
14 speed by which the BH wanders around the center is small, $\sim (m_* / M_{\text{BH}})^{1/2} \sigma_*$, where m_* and
15 M_{BH} are the masses of a single star and the BH, respectively, and σ_* is the stellar velocity
16 dispersion. Since the random force fluctuates on a dynamical time, the BH wanders across a region
17 that is smaller by a factor of $\sim (m_* / M_{\text{BH}})^{1/2}$ than the region traversed by the stars inducing the
18 fluctuating force on it.

19
20 The dynamical insignificance of the BH on the global galactic scale is misleading. The gravitational
21 binding energy per rest-mass energy of galaxies is of order $\sim (\sigma_* / c)^2 < 10^{-6}$. Since BH are
22 relativistic objects, the gravitational binding energy of material that feeds them amounts to a
23 substantial fraction its rest mass energy. Even if the BH mass amounts to a fraction as small as
24 $\sim 10^{-4}$ of the baryonic mass in a galaxy, and only a percent of the accreted rest-mass energy is
25 deposited into the gaseous environment of the BH, this slight deposition can unbind the entire gas
26 reservoir of the host galaxy. This order-of-magnitude estimate explains why quasars may be short
27 lived. As soon as the central BH accretes large quantities of gas so as to significantly increase its
28 mass, it releases large amounts of energy and momentum that could suppress further accretion onto
29 it. In short, the BH growth might be *self-regulated*.

30
31 The principle of *self-regulation* naturally leads to a correlation between the final BH mass, M_{bh} ,
32 and the depth of the gravitational potential well to which the surrounding gas is confined. The latter
33 can be characterized by the velocity dispersion of the associated stars, $\sim \sigma_*^2$. Indeed a correlation
34 between M_{bh} and σ_*^4 is observed in the present-day Universe. If quasars shine near their
35 Eddington limit as suggested by observations of low and high-redshift quasars, then a fraction of
36 $\sim 5-10\%$ of the energy released by the quasar over a galactic dynamical time needs to be
37 captured in the surrounding galactic gas in order for the BH growth to be self-regulated (see Figure
38 10). With this interpretation, the $M_{\text{bh}} - \sigma_*$ relation reflects the limit introduced to the BH mass by
39 self-regulation; deviations from this relation are inevitable during episodes of BH growth or as a
40 result of mergers of galaxies that have no cold gas in them. A physical scatter around this upper
41 envelope could also result from variations in the efficiency by which the released BH energy
42 couples to the surrounding gas.

43
44 Figure 10. Simulation images of a merger of galaxies resulting in quasar activity that eventually
45 shuts-off the accretion of gas onto the black hole (from Di Matteo et al. 2005). The upper (lower)

panels show a sequence of snapshots of the gas distribution during a merger with (without) feedback from a central black hole. The temperature of the gas is color coded.

Various prescriptions for self-regulation were sketched in the literature. These involve either energy or momentum-driven winds, with the latter type being a factor of $\sim v_c / c$ less efficient. The quasar remains active during the dynamical time of the initial gas reservoir, $\sim 10^7$ years, and fades afterwards due to the dilution of this reservoir. The BH growth may resume if the cold gas reservoir is replenished through a new merger. Following early analytic work, extensive numerical simulations demonstrated that galaxy mergers do produce the observed correlations between black hole mass and spheroid properties. Because of the limited resolution near the galaxy nucleus, these simulations adopt a simple prescription for the accretion flow that feeds the black hole. The actual feedback in reality may depend crucially on the geometry of this flow and the physical mechanism that couples the energy or momentum output of the quasar to the surrounding gas.

The inflow of cold gas towards galaxy centers during the growth phase of the BH would naturally be accompanied by a burst of star formation. The fraction of gas that is not consumed by stars or ejected by supernova-driven winds, will continue to feed the BH. It is therefore not surprising that quasar and starburst activities co-exist in Ultra Luminous Infrared Galaxies, and that all quasars show broad metal lines indicating pre-enrichment of the surrounding gas with heavy elements.

The upper mass of galaxies may also be regulated by the energy output from quasar activity. This would account for the fact that cooling flows are suppressed in present-day X-ray clusters, and that massive BHs and stars in galactic bulges were already formed at $z \sim 2$. In the cores of cooling X-ray clusters, there is often an active central BH that supplies sufficient energy to compensate for the cooling of the gas. The primary physical process by which this energy couples to the gas is still unknown.

The quasars discovered so far at $z \sim 6$ mark the early growth of the most massive BHs and galactic spheroids. The BHs powering these bright quasars possess a mass of a few billion solar masses. A quasar radiating at its Eddington limiting luminosity, $L_E = 1.4 \times 10^{47} \text{ erg s}^{-1} (M_{\text{bh}} / 10^9 M_\odot)$, with a radiative efficiency, $\varepsilon_{\text{rad}} = L_E / \dot{M} c^2$, for converting accreted mass into radiation, would grow exponentially in mass as a function of time t , $M_{\text{bh}} = M_{\text{seed}} \exp\{t / t_E\}$ from its initial seed mass M_{seed} , on a time scale, $t_E = 4.1 \times 10^7 \text{ yr} (\varepsilon_{\text{rad}} / 0.1)$. Thus, the required growth time in units of the Hubble time $t_{\text{hubble}} = 10^9 \text{ yr} [(1+z)/7]^{-3/2}$ is

$$\frac{t_{\text{growth}}}{t_{\text{hubble}}} = 0.7 \left(\frac{\varepsilon_{\text{rad}}}{10\%} \right) \left(\frac{1+z}{7} \right)^{3/2} \ln \left(\frac{M_{\text{bh}} / 10^9 M_\odot}{M_{\text{seed}} / 100 M_\odot} \right). \quad (28)$$

The age of the Universe at $z \sim 6$ provides just sufficient time to grow a BH with $M_{\text{bh}} \sim 10^9 M_\odot$ out of a stellar mass seed with $\varepsilon_{\text{rad}} = 10\%$. The growth time is shorter for smaller radiative efficiencies or a higher seed mass.

2.6. The Epoch of Reionization

1 Given the understanding described above of how many galaxies formed at various times, the course
2 of reionization can be determined universe-wide by counting photons from all sources of light. Both
3 stars and black holes contribute ionizing photons, but the early universe is dominated by small
4 galaxies which in the local universe have central black holes that are disproportionately small, and
5 indeed quasars are rare above redshift 6. Thus, stars most likely dominated the production of
6 ionizing UV photons during the reionization epoch [although high-redshift galaxies should have
7 also emitted X-rays from accreting black holes and accelerated particles in collisionless shocks].
8 Since most stellar ionizing photons are only slightly more energetic than the 13.6 eV ionization
9 threshold of hydrogen, they are absorbed efficiently once they reach a region with substantial
10 neutral hydrogen). This makes the IGM during reionization a two-phase medium characterized by
11 highly ionized regions separated from neutral regions by sharp ionization fronts (see Figure 11).

12
13 Figure 11. The spatial structure of cosmic reionization. The illustration shows how regions with
14 large-scale overdensities form large concentrations of galaxies (dots) whose ionizing photons
15 produce enormous joint ionized bubbles (upper left). At the same time, galaxies are rare within
16 large-scale voids, in which the IGM is still mostly neutral (lower right).

17
18 We can obtain a first estimate of the requirements of reionization by demanding one stellar ionizing
19 photon for each hydrogen atom in the IGM. If we conservatively assume that stars within the early
20 galaxies were similar to those observed locally, then each star produced ~ 4000 ionizing photons
21 per baryon. Star formation is observed today to be an inefficient process, but even if stars in
22 galaxies formed out of only $\sim 10\%$ of the available gas, it was still sufficient to accumulate a small
23 fraction (of order 0.1%) of the total baryonic mass in the universe into galaxies in order to ionize
24 the entire IGM. More accurate estimates of the actual required fraction account for the formation of
25 some primordial stars (which were massive, efficient ionizers, as discussed above), and for
26 recombinations of hydrogen atoms at high redshifts and in dense regions.

27
28 From studies of quasar absorption lines at $z \sim 6$ we know that the IGM is highly ionized a billion
29 years after the big bang. There are hints, however, that some large neutral hydrogen regions persist
30 at these early times and so this suggests that we may not need to go to much higher redshifts to
31 begin to see the epoch of reionization. We now know that the universe could not have fully
32 reionized earlier than an age of 300 million years, since WMAP observed the effect of the freshly
33 created plasma at reionization on the large-scale polarization anisotropies of the CMB and this
34 limits the reionization redshift; an earlier reionization, when the universe was denser, would have
35 created a stronger scattering signature that would be inconsistent with the WMAP observations. In
36 any case, the redshift at which reionization ended only constrains the overall cosmic efficiency of
37 ionizing photon production. In comparison, a detailed picture of reionization as it happens will
38 teach us a great deal about the population of young galaxies that produced this cosmic phase
39 transition. A key point is that the spatial distribution of ionized bubbles is determined by clustered
40 groups of galaxies and not by individual galaxies. At such early times galaxies were strongly
41 clustered even on very large scales (up to tens of Mpc), and these scales therefore dominate the
42 structure of reionization. The basic idea is simple. At high redshift, galactic halos are rare and
43 correspond to rare, high density peaks. As an analogy, imagine searching on Earth for mountain
44 peaks above 5000 meters. The 200 such peaks are not at all distributed uniformly but instead are
45 found in a few distinct clusters on top of large mountain ranges. Given the large-scale boost
46 provided by a mountain range, a small-scale crest need only provide a small additional rise in order
47 to become a 5000 meter peak. The same crest, if it formed within a valley, would not come
48 anywhere near 5000 meters in total height. Similarly, in order to find the early galaxies, one must
49 first locate a region with a large-scale density enhancement, and then galaxies will be found there in
50 abundance.

1 The ionizing radiation emitted from the stars in each galaxy initially produces an isolated ionized
2 bubble. However, in a region dense with galaxies the bubbles quickly overlap into one large bubble,
3 completing reionization in this region while the rest of the universe is still mostly neutral
4 (Figure 11). Most importantly, since the abundance of rare density peaks is very sensitive to small
5 changes in the density threshold, even a large-scale region with a small enhanced density (say, 10%
6 above the mean density of the universe) can have a much larger concentration of galaxies than in
7 other regions (e.g., a 50% enhancement). On the other hand, reionization is harder to achieve in
8 dense regions, since the protons and electrons collide and recombine more often in such regions,
9 and newly-formed hydrogen atoms need to be reionized again by additional ionizing photons.
10 However, the overdense regions end up reionizing first since the number of ionizing sources in
11 these regions is increased so strongly. The large-scale topology of reionization is therefore inside
12 out, with underdense voids reionizing only at the very end of reionization, with the help of extra
13 ionizing photons coming in from their surroundings (which have a higher density of galaxies than
14 the voids themselves). This is a key prediction awaiting observational testing.

15
16 Detailed analytical models that account for large-scale variations in the abundance of galaxies
17 confirm that the typical bubble size starts well below a Mpc early in reionization, as expected for an
18 individual galaxy, rises to 5–10 Mpc during the central phase (i.e., when the universe is half
19 ionized), and then by another factor of ~ 5 towards the end of reionization. These scales are given
20 in comoving units that scale with the expansion of the universe, so that the actual sizes at a redshift
21 z were smaller than these numbers by a factor of $1 + z$. Numerical simulations have only recently
22 begun to reach the enormous scales needed to capture this evolution. Accounting precisely for
23 gravitational evolution on a wide range of scales but still crudely for gas dynamics, star formation,
24 and the radiative transfer of ionizing photons, the simulations confirm that the large-scale topology
25 of reionization is inside out, and that this topology can be used to study the abundance and
26 clustering of the ionizing sources (Figure 11).

27
28 The characteristic observable size of the ionized bubbles at the end reionization can be calculated
29 based on simple considerations that only depend on the power-spectrum of density fluctuations and
30 the redshift. As the size of an ionized bubble increases, the time it takes a 21-cm photon emitted by
31 hydrogen to traverse it gets longer. At the same time, the variation in the time at which different
32 regions reionize becomes smaller as the regions grow larger. Thus, there is a maximum size above
33 which the photon crossing time is longer than the cosmic variance in ionization time. Regions
34 bigger than this size will be ionized at their near side by the time a 21-cm photon will cross them
35 towards the observer from their far side. They would appear to the observer as one-sided, and hence
36 signal the end of reionization. These considerations imply a characteristic size for the ionized
37 bubbles of ~ 10 physical Mpc at $z \sim 6$ (equivalent to 70 Mpc today). This result implies that
38 future radio experiments should be tuned to a characteristic angular scale of tens of arcminutes for
39 an optimal detection of 21-cm brightness fluctuations near the end of reionization (see [Section 3.2](#)).

Deleted: §

40 41 **2.7. Post-Reionization Suppression of Low-Mass Galaxies**

42
43 After the ionized bubbles overlapped in each region, the ionizing background increased sharply, and
44 the IGM was heated by the ionizing radiation to a temperature $T_{\text{IGM}} > 10^4$ K. Due to the
45 substantial increase in the IGM pressure, the smallest mass scale into which the cosmic gas could
46 fragment, the so-called Jeans mass, increased dramatically, changing the minimum mass of forming
47 galaxies.

48
49 Gas infall depends sensitively on the Jeans mass. When a halo more massive than the Jeans mass
50 begins to form, the gravity of its dark matter overcomes the gas pressure. Even in halos below the
51 Jeans mass, although the gas is initially held up by pressure, once the dark matter collapses its

1 increased gravity pulls in some gas. Thus, the Jeans mass is generally higher than the actual limiting
 2 mass for accretion. Before reionization, the IGM is cold and neutral, and the Jeans mass plays a
 3 secondary role in limiting galaxy formation compared to cooling. After reionization, the Jeans mass
 4 is increased by several orders of magnitude due to the photoionization heating of the IGM, and
 5 hence begins to play a dominant role in limiting the formation of stars. Gas infall in a reionized and
 6 heated Universe has been investigated in a number of numerical simulations. Three dimensional
 7 numerical simulations found a significant suppression of gas infall in even larger halos
 8 ($V_c \sim 75 \text{ km s}^{-1}$), but this was mostly due to a suppression of late infall at $z < 2$.

9
 10 When a volume of the IGM is ionized by stars, the gas is heated to a temperature $T_{\text{IGM}} \sim 10^4$ K. If
 11 quasars dominate the UV background at reionization, their harder photon spectrum leads to
 12 $T_{\text{IGM}} > 2 \times 10^4$ K. Including the effects of dark matter, a given temperature results in a linear
 13 Jeans mass corresponding to a halo circular velocity of

$$15 \quad V_J \approx 80 \left(\frac{T_{\text{IGM}}}{1.5 \times 10^4 \text{ K}} \right)^{1/2} \text{ km s}^{-1}. \quad (29)$$

16
 17 In halos with a circular velocity well above V_J , the gas fraction in infalling gas equals the universal
 18 mean of Ω_b / Ω_m , but gas infall is suppressed in smaller halos. A simple estimate of the limiting
 19 circular velocity, below which halos have essentially no gas infall, is obtained by substituting the
 20 virial overdensity for the mean density in the definition of the Jeans mass. The resulting estimate is

$$22 \quad V_{\text{lim}} = 34 \left(\frac{T_{\text{IGM}}}{1.5 \times 10^4 \text{ K}} \right)^{1/2} \text{ km s}^{-1}. \quad (30)$$

23
 24 This value is in rough agreement with the numerical simulations mentioned before.

25
 26 Although the Jeans mass is closely related to the rate of gas infall at a given time, it does not
 27 directly yield the total gas residing in halos at a given time. The latter quantity depends on the entire
 28 history of gas accretion onto halos, as well as on the merger histories of halos, and an accurate
 29 description must involve a time-averaged Jeans mass. The gas content of halos in simulations is
 30 well fit by an expression which depends on the filtering mass, a particular time-averaged Jeans
 31 mass.

32
 33 The reionization process was not perfectly synchronized throughout the Universe. Large-scale
 34 regions with a higher density than the mean tended to form galaxies first and reionized earlier than
 35 underdense regions. The suppression of low-mass galaxies by reionization is therefore modulated
 36 by the fluctuations in the timing of reionization. Inhomogeneous reionization imprint is a signature
 37 on the power-spectrum of low-mass galaxies. Future high-redshift galaxy surveys hoping to
 38 constrain inflationary parameters must properly model the effects of reionization; conversely, they
 39 will also place new constraints on the thermal history of the IGM during reionization.

41 3. Probing the Diffuse Intergalactic Hydrogen

42 3.1. Lyman-Alpha Absorption

43
 44

Resonant Lyman- α absorption has thus far proved to be the best probe of the state of the IGM. The optical depth to absorption by a uniform intergalactic medium is

$$\tau_s = \frac{\pi e^2 f_\alpha \lambda_\alpha n_{\text{HI}}(z)}{m_e c H(z)} \quad (31)$$

$$\approx 6.45 \times 10^5 x_{\text{HI}} \left(\frac{\Omega_b h}{0.0315} \right) \left(\frac{\Omega_m}{0.3} \right)^{-1/2} \left(\frac{1+z}{10} \right)^{3/2},$$

where $H \approx 100h \text{ km s}^{-1} \text{ Mpc}^{-1} \Omega_m^{1/2} (1+z)^{3/2}$ is the Hubble parameter at redshift z ; $f_\alpha = 0.4162$ and $\lambda_\alpha = 1216 \text{ \AA}$ are the oscillator strength and wavelength of the Lyman- α transition; $n_{\text{HI}}(z)$ is the neutral hydrogen density at z (assuming primordial abundances); Ω_m and Ω_b are the present-day density parameters of all matter and of baryons, respectively; and x_{HI} is the average fraction of neutral hydrogen. In the second equality we have implicitly considered high redshifts.

Deleted: are the oscillator s
Deleted:

Figure 12. Using Lyman- α absorption in quasar spectra to probe the ionization state of the IGM.

This figure from White et al. (2003) shows the observed spectrum of a $z = 6.28$ quasar (solid curve), and the expected unabsorbed emission (dashed curve), based on an average over many quasars seen at lower redshifts. The unabsorbed emission is a sum of smooth emission (the “continuum”, dotted curve) plus emission features from atomic resonances (“emission lines”).

Lyman- α absorption is thus highly sensitive to the presence of even trace amounts of neutral hydrogen. The lack of full absorption in quasar spectra then implies that the IGM has been very highly ionized during much of the history of the universe, from at most a billion years after the big bang to the present time. At redshifts approaching six, however, the optical depth increases, and the observed absorption becomes very strong. An example of this is shown in Figure 12, where an observed quasar spectrum is compared to the unabsorbed expectation for the same quasar. The prominent Lyman- α emission line, which is produced by radiating hot gas near the quasar itself, is centered at a wavelength of 8850 \AA , which for the redshift (6.28) of this quasar corresponds to a rest-frame 1216 \AA . Above this wavelength, the original emitted quasar spectrum is seen, since photons emitted with wavelengths higher than 1216 \AA redshift to higher wavelengths during their journey toward us and never encounter resonance lines of hydrogen atoms. Shorter-wavelength photons, however, redshift until they hit the local 1216 \AA and are then absorbed by any existing hydrogen atoms. The difference between the unabsorbed expectation and the actual observed spectrum can be used to measure the amount of absorption, and thus to infer the atomic hydrogen density. For this particular quasar, this difference is very large (i.e., the observed flux is near zero) just to the blue of the Lyman- α emission line.

Deleted: α

Deleted: α

Figure 13. Spectra of 19 quasars with redshifts $5.74 < z < 6.42$ from the *Sloan Digital Sky Survey*, taken from Fan et al. (2005). For some of the highest-redshift quasars, the spectrum shows no transmitted flux shortward of the Lyman- α wavelength at the quasar redshift (the so-called “Gunn-Peterson trough”), indicating a non-negligible neutral fraction in the IGM.

Several quasars beyond $z \sim 6.1$ show in their spectra such a (so-called “Gunn-Peterson”) trough, a

Deleted:

1 blank spectral region at wavelengths shorter than Ly α at the quasar redshift (Figure 13). The
 2 detection of Gunn-Peterson troughs indicates a rapid change in the neutral content of the IGM at
 3 $z \sim 6$, and hence a rapid change in the intensity of the background ionizing flux. However, even a
 4 small atomic hydrogen fraction of $\sim 10^{-3}$ would still produce nearly complete Ly α absorption.

5
 6 While only resonant Ly α absorption is important at moderate redshifts, the damping wing of the
 7 Ly α line plays a significant role when neutral fractions of order unity are considered at $z > 6$. The
 8 scattering cross-section of the Ly α resonance line by neutral hydrogen is given by

$$9 \quad \sigma_{\alpha}(\nu) = \frac{3\lambda_{\alpha}^2 \Lambda_{\alpha}^2}{8\pi} \frac{(\nu/\nu_{\alpha})^4}{4\pi^2(\nu-\nu_{\alpha})^2 + (\Lambda_{\alpha}^2/4)(\nu/\nu_{\alpha})^6}, \quad (32)$$

11
 12 where $\Lambda_{\alpha} = (8\pi^2 e^2 f_{\alpha} / 3m_e c \lambda_{\alpha}^2) = 6.25 \times 10^8 \text{ s}^{-1}$ is the Ly α ($2p \rightarrow 1s$) decay rate,
 13 $f_{\alpha} = 0.4162$ is the oscillator strength, and $\lambda_{\alpha} = 1216 \text{ \AA}$ and $\nu_{\alpha} = (c / \lambda_{\alpha}) = 2.47 \times 10^{15} \text{ Hz}$
 14 are the wavelength and frequency of the Ly α line. The term in the numerator is responsible for the
 15 classical Rayleigh scattering.

16
 17 Although reionization is an inhomogeneous process, we consider here a simple illustrative case of
 18 instantaneous reionization. Consider a source at a redshift z_s beyond the redshift of reionization,
 19 z_{reion} , and the corresponding scattering optical depth of a uniform, neutral IGM of hydrogen
 20 density $n_{\text{H},0}(1+z)^3$ between the source and the reionization redshift. The optical depth is a
 21 function of the observed wavelength λ_{obs} ,

$$22 \quad \tau(\lambda_{\text{obs}}) = \int_{z_{\text{reion}}}^{z_s} dz \frac{cdt}{dz} n_{\text{H},0}(1+z)^3 \sigma_{\alpha}[\nu_{\text{obs}}(1+z)], \quad (33)$$

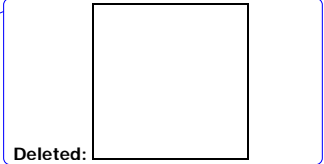
24
 25 where $\nu_{\text{obs}} = c / \lambda_{\text{obs}}$ and

$$26 \quad \frac{dt}{dz} = [(1+z)H(z)]^{-1} = H_0^{-1} \times \left[\Omega_m(1+z)^5 + \Omega_{\Lambda}(1+z)^2 + (1-\Omega_m-\Omega_{\Lambda})(1+z)^4 \right]^{-1/2}. \quad (34)$$

27
 28 At wavelengths longer than Ly α at the source, the optical depth obtains a small value; these
 29 photons redshift away from the line center along its red wing and never resonate with the line core
 30 on their way to the observer. Considering only the regime in which $|\nu - \nu_{\alpha}| \gg \Lambda_{\alpha}$, we may ignore
 31 the second term in the denominator of equation (32). This leads to an analytical result for the red
 32 damping wing of the Gunn-Peterson trough,

$$33 \quad \tau(\lambda_{\text{obs}}) = \tau_s \left(\frac{\Lambda}{4\pi^2 \nu_{\alpha}} \right) \tilde{\lambda}_{\text{obs}}^{3/2} \left[I(\tilde{\lambda}_{\text{obs}}^{-1}) - I([(1+z_{\text{reion}})/(1+z_s)]\tilde{\lambda}_{\text{obs}}^{-1}) \right], \quad (35)$$

35
 36 an expression valid for $\tilde{\lambda}_{\text{obs}} \geq 1$, where τ_s is given in equation (31), and we also define



Deleted:

Deleted: α

Deleted: α

Deleted: α

Deleted: α

Deleted: α

Deleted: and

Deleted: α

Comment [R2]: Size reduced to accommodate the period at the end of the equation.

Deleted:)

Deleted: α

$$\tilde{\lambda}_{\text{obs}} \equiv \frac{\lambda_{\text{obs}}}{(1+z_s)\lambda_\alpha} \quad (36)$$

and

$$I(x) \equiv \frac{x^{9/2}}{1-x} + \frac{9}{7}x^{7/2} + \frac{9}{5}x^{5/2} + 3x^{3/2} + 9x^{1/2} - \frac{9}{2} \ln \left[\frac{1+x^{1/2}}{1-x^{1/2}} \right]. \quad (37)$$

At wavelengths shorter than 912\AA , the photons are absorbed when they photoionize atoms of hydrogen or helium. The bound-free absorption cross-section from the ground state of a hydrogenic ion with nuclear charge Z and an ionization threshold $h\nu_0$, is given by

$$\sigma_{\text{bf}}(\nu) = \frac{6.30 \times 10^{-18}}{Z^2} \text{cm}^2 \times \left(\frac{\nu_0}{\nu} \right)^4 \frac{e^{4-(4 \tan^{-1} \varepsilon)/\varepsilon}}{1 - e^{-2\pi/\varepsilon}} \quad \text{for } \nu \geq \nu_0, \quad (38)$$

where $\varepsilon \equiv \sqrt{(\nu/\nu_0) - 1}$. For neutral hydrogen, $Z=1$ and $\nu_{\text{H},0} = (c/\lambda_c) = 3.29 \times 10^{15} \text{ Hz}$ ($h\nu_{\text{H},0} = 13.60 \text{ eV}$); for singly-ionized helium, $Z=2$ and $\nu_{\text{He II},0} = 1.31 \times 10^{16} \text{ Hz}$ ($h\nu_{\text{He II},0} = 54.42 \text{ eV}$). The cross-section for neutral helium is more complicated; when averaged over its narrow resonances it can be fitted to an accuracy of a few percent up to $h\nu = 50 \text{ keV}$ by the fitting function

$$\sigma_{\text{bf,He I}}(\nu) = 9.492 \times 10^{-16} \text{ cm}^2 \times \left[(x-1)^2 + 4.158 \right] y^{-1.953} \left(1 + 0.825 y^{1/4} \right)^{-3.188}, \quad (39)$$

where $x \equiv [(\nu/3.286 \times 10^{15} \text{ Hz}) - 0.4434]$, $y \equiv x^2 + 4.563$, and the threshold for ionization is $\nu_{\text{He I},0} = 5.938 \times 10^{15} \text{ Hz}$ ($h\nu_{\text{He I},0} = 24.59 \text{ eV}$).

For rough estimates, the average photoionization cross-section for a mixture of hydrogen and helium with cosmic abundances can be approximated in the range of $54 < h\nu < 10^3 \text{ eV}$ as $\sigma_{\text{bf}} \approx \sigma_0 (\nu/\nu_{\text{H},0})^{-3}$, where $\sigma_0 \approx 6 \times 10^{-17} \text{ cm}^2$. The redshift factor in the cross-section then cancels exactly the redshift evolution of the gas density and the resulting optical depth depends only on the elapsed cosmic time, $t(z_{\text{reion}}) - t(z_s)$. At high redshifts this yields

$$\tau_{\text{bf}}(\lambda_{\text{obs}}) = \int_{z_{\text{reion}}}^{z_s} dz \frac{cdt}{dz} n_0 (1+z)^3 \sigma_{\text{bf}}[\nu_{\text{obs}}(1+z)]$$

$$\approx 1.5 \times 10^2 \left(\frac{\Omega_b h}{0.03} \right) \left(\frac{\Omega_m}{0.3} \right)^{-1/2} \left(\frac{\lambda}{100\text{\AA}} \right)^3 \times \left[\frac{1}{(1+z_{\text{reion}})^{3/2}} - \frac{1}{(1+z_s)^{3/2}} \right]. \quad (40)$$

The bound-free optical depth only becomes of order unity in the extreme ultraviolet (UV) to soft X-rays, around $h\nu \sim 0.1$ keV, a regime which is unfortunately difficult to observe due to Galactic absorption.

3.2. 21-cm Absorption or Emission

3.2.1. The Spin Temperature of the 21-cm Transition of Hydrogen

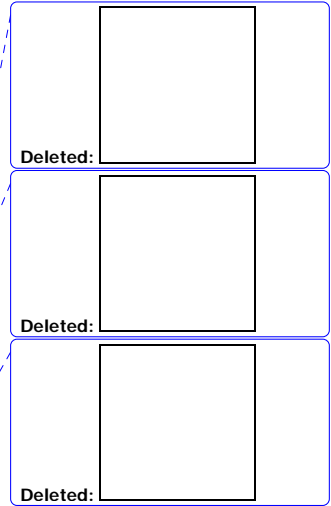
The ground state of hydrogen exhibits hyperfine splitting owing to the possibility of two relative alignments of the spins of the proton and the electron. The state with parallel spins (the triplet state) has a slightly higher energy than the state with anti-parallel spins (the singlet state). The 21-cm line associated with the spin-flip transition from the triplet to the singlet state is often used to detect neutral hydrogen in the local universe. At high redshift, the occurrence of a neutral pre-reionization IGM offers the prospect of detecting the first sources of radiation and probing the reionization era by mapping the 21-cm emission from neutral regions. While its energy density is estimated to be only a 1% correction to that of the CMB, the redshifted 21-cm emission should display angular structure as well as frequency structure due to inhomogeneities in the gas density field, hydrogen ionized fraction, and spin temperature. Indeed, a full mapping of the distribution of H I as a function of redshift is possible in principle.

The basic physics of the hydrogen spin transition is determined as follows. The ground-state hyperfine levels of hydrogen tend to thermalize with the CMB background, making the IGM unobservable. If other processes shift the hyperfine level populations away from thermal equilibrium, then the gas becomes observable against the CMB in emission or in absorption. The relative occupancy of the spin levels is usually described in terms of the hydrogen spin temperature T_S , defined by

$$\frac{n_1}{n_0} = 3 \exp\left\{-\frac{T_*}{T_S}\right\}, \quad (41)$$

where n_0 and n_1 refer respectively to the singlet and triplet hyperfine levels in the atomic ground state ($n=1$), and $T_* = 0.068$ K is defined by $k_B T_* = E_{21}$, where the energy of the 21 cm transition is $E_{21} = 5.9 \times 10^{-6}$ eV, corresponding to a frequency of 1420 MHz. In the presence of the CMB alone, the spin states reach thermal equilibrium with $T_S = T_{\text{CMB}} = 2.725(1+z)$ K on a time-scale of $\tau = T_*/(T_{\text{CMB}} A_{10}) \approx 3 \times 10^5 (1+z)^{-1}$ yr, where $A_{10} = 2.87 \times 10^{-15} \text{ s}^{-1}$ is the spontaneous decay rate of the hyperfine transition. This time-scale is much shorter than the age of the universe at all redshifts after cosmological recombination.

The IGM is observable when the kinetic temperature T_k of the gas differs from T_{CMB} and an effective mechanism couples T_S to T_k . Collisional de-excitation of the triplet level dominates at very high redshift, when the gas density (and thus the collision rate) is still high, but once a significant galaxy population forms in the universe, the spin temperature is affected also by an indirect mechanism that acts through the scattering of Lyman- α photons. Continuum UV photons produced by early radiation sources redshift by the Hubble expansion into the local Lyman- α line at a lower redshift. These photons mix the spin states via the Wouthuysen-Field process whereby an



1 atom initially in the $n=1$ state absorbs a Lyman- α photon, and the spontaneous decay which
 2 returns it from $n=2$ to $n=1$ can result in a final spin state which is different from the initial one.
 3 Since the neutral IGM is highly opaque to resonant scattering, and the Lyman- α photons receive
 4 Doppler kicks in each scattering, the shape of the radiation spectrum near Lyman- α is determined
 5 by T_k (Field 1959), and the resulting spin temperature (assuming $T_S \gg T_*$) is then a weighted
 6 average of T_k and T_{CMB} :

$$8 \quad T_S = \frac{T_{\text{CMB}} T_k (1 + x_{\text{tot}})}{T_k + T_{\text{CMB}} x_{\text{tot}}}, \quad (42)$$

9
 10 where $x_{\text{tot}} = x_\alpha + x_c$ is the sum of the radiative and collisional threshold parameters. These
 11 parameters are

$$13 \quad x_\alpha = \frac{P_{10} T_*}{A_{10} T_{\text{CMB}}}, \quad (43)$$

14 and

$$16 \quad x_c = \frac{4\kappa_{1-0}(T_k) n_{\text{H}} T_*}{3A_{10} T_{\text{CMB}}}, \quad (44)$$

17
 18 where P_{10} is the indirect de-excitation rate of the triplet $n=1$ state via the Wouthuysen-Field
 19 process, related to the total scattering rate P_α of Lyman- α photons by $P_{10} = 4P_\alpha / 27$. Also, the
 20 atomic coefficient $\kappa_{1-0}(T_k)$ is tabulated as a function of T_k . The coupling of the spin temperature
 21 to the gas temperature becomes substantial when $x_{\text{tot}} > 1$; in particular, $x_\alpha = 1$ defines the
 22 thermalization rate of P_α :

$$24 \quad P_{\text{th}} \equiv \frac{27A_{10} T_{\text{CMB}}}{4T_*} \simeq 7.6 \times 10^{-12} \left(\frac{1+z}{10} \right) \text{s}^{-1}. \quad (45)$$

25
 26 A patch of neutral hydrogen at the mean density and with a uniform T_S produces (after correcting
 27 for stimulated emission) an optical depth at a present-day (observed) wavelength of $21(1+z)$ cm,

$$29 \quad \tau(z) = 9.0 \times 10^{-3} \left(\frac{T_{\text{CMB}}}{T_S} \right) \left(\frac{\Omega_b h}{0.03} \right) \left(\frac{\Omega_m}{0.3} \right)^{-1/2} \left(\frac{1+z}{10} \right)^{1/2}, \quad (46)$$

30
 31 assuming a high redshift $z \gg 1$. The observed spectral intensity I_ν relative to the CMB at a
 32 frequency ν is measured by radio astronomers as an effective brightness temperature T_b of
 33 blackbody emission at this frequency, defined using the Rayleigh-Jeans limit of the Planck radiation

Deleted:

Deleted:

Deleted:

Deleted:

Deleted:

Deleted:

1 formula: $I_\nu \equiv 2k_B T_b \nu^2 / c^2$.

2
3 The brightness temperature through the IGM is $T_b = T_{\text{CMB}} e^{-\tau} + T_S (1 - e^{-\tau})$, so the observed
4 differential antenna temperature of this region relative to the CMB is

5
6
$$T_b = (1+z)^{-1} (T_S - T_{\text{CMB}}) (1 - e^{-\tau})$$

7
8
$$\approx 28 \text{ mK} \left(\frac{\Omega_b h}{0.033} \right) \left(\frac{\Omega_m}{0.27} \right)^{-1/2} \left(\frac{1+z}{10} \right)^{1/2} \left(\frac{T_S - T_{\text{CMB}}}{T_S} \right), \quad (47)$$

9
10 where $\tau \ll 1$ is assumed and T_b has been redshifted to redshift zero. Note that the combination
11 that appears in T_b is

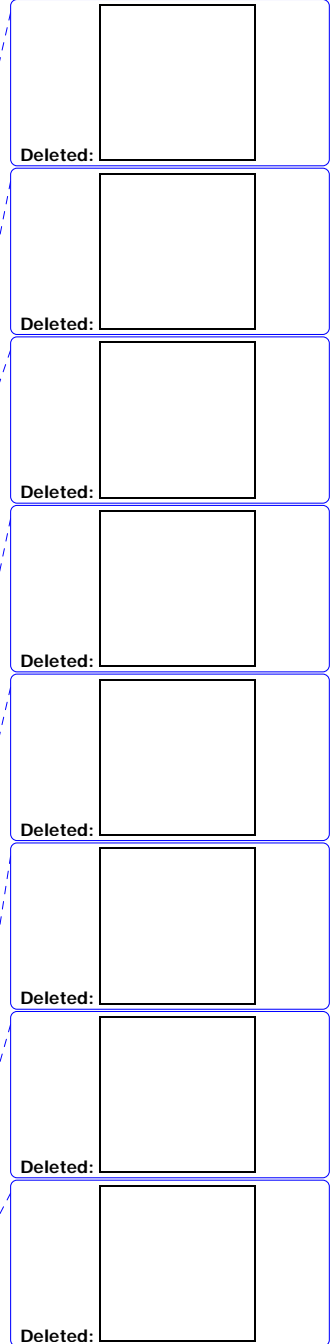
12
13
$$\frac{T_S - T_{\text{CMB}}}{T_S} = \frac{x_{\text{tot}}}{1 + x_{\text{tot}}} \left(1 - \frac{T_{\text{CMB}}}{T_k} \right). \quad (48)$$

14
15 In overdense regions, the observed T_b is proportional to the overdensity, and in partially ionized
16 regions T_b is proportional to the neutral fraction. Also, if $T_S \gg T_{\text{CMB}}$ then the IGM is observed in
17 emission at a level that is independent of T_S . On the other hand, if $T_S \ll T_{\text{CMB}}$ then the IGM is
18 observed in absorption at a level that is enhanced by a factor of T_{CMB} / T_S . As a result, a number of
19 cosmic events are expected to leave observable signatures in the redshifted 21-cm line, as discussed
20 below in further detail.

21
22 Figure 14. *Top panel:* Evolution with redshift z of the CMB temperature T_{CMB} (dotted curve), the
23 gas kinetic temperature T_k (dashed curve), and the spin temperature T_S (solid curve), taken from
24 Pritchard & Loeb (2008). *Middle panel:* Evolution of the gas fraction in ionized regions x_i (solid
25 curve) and the ionized fraction outside these regions (due to diffuse X-rays) x_e (dotted curve).
26 *Bottom panel:* Evolution of mean 21 cm brightness temperature T_b . The horizontal axis at the top
27 provides the observed photon frequency at the different redshifts shown at the bottom. Each panel
28 shows curves for three models in which reionization is completed at different redshifts, namely
29 $z = 6.47$ (thin curves), $z = 9.76$ (medium curves), and $z = 11.76$ (thick curves).

30
31 Figure 14 illustrates the mean IGM evolution for three examples in which reionization is completed
32 at different redshifts, namely $z = 6.47$ (thin curves), $z = 9.76$ (medium curves), and $z = 11.76$
33 (thick curves). The top panel shows the global evolution of the CMB temperature T_{CMB} (dotted
34 curve), the gas kinetic temperature T_k (dashed curve), and the spin temperature T_S (solid curve).
35 The middle panel shows the evolution of the ionized gas fraction and the bottom panel presents the
36 mean 21 cm brightness temperature, T_b .

37



3.2.2. A Handy Tool for Studying Cosmic Reionization

The prospect of studying reionization by mapping the distribution of atomic hydrogen across the universe using its prominent 21-cm spectral line has motivated several teams to design and construct arrays of low-frequency radio telescopes; the Low Frequency Array (<http://www.lofar.org/>), the Mileura Wide-Field Array (<http://www.haystack.mit.edu/ast/arrays/mwa/site/index.html>), the Primeval Structure Telescope (<http://arxiv.org/abs/astro-ph/0502029>), and ultimately the Square Kilometer Array (<http://www.skatelescope.org>) will search over the next decade for 21-cm emission or absorption from $z \sim 6.5 - 15$, redshifted and observed today at relatively low frequencies which correspond to wavelengths of 1.5 to 4 meters.

Formatted: Font: Not Italic, No underline, Font color: Auto

Formatted: Font: Not Italic

Formatted: Font: Not Italic

Formatted: Font: Not Italic

The idea is to use the resonance associated with the hyperfine splitting in the ground state of hydrogen. While the CMB spectrum peaks at a wavelength of 2 mm, it provides a still-measurable intensity at meter wavelengths that can be used as the bright background source against which we can see the expected 1% absorption by neutral hydrogen along the line of sight. The hydrogen gas produces 21-cm absorption if its spin temperature is colder than the CMB and excess emission if it is hotter. Since the CMB covers the entire sky, a complete three-dimensional map of neutral hydrogen can in principle be made from the sky position of each absorbing gas cloud together with its redshift z . Different observed wavelengths slice the Universe at different redshifts, and ionized regions are expected to appear as cavities in the hydrogen distribution, similar to holes in Swiss cheese. Because the smallest angular size resolvable by a telescope is proportional to the observed wavelength, radio astronomy at wavelengths as large as a meter has remained relatively undeveloped. Producing resolved images even of large sources such as cosmological ionized bubbles requires telescopes which have a kilometer scale. It is much more cost-effective to use a large array of thousands of simple antennas distributed over several kilometers, and to use computers to cross-correlate the measurements of the individual antennas and combine them effectively into a single large telescope. The new experiments are being placed mostly in remote sites, because the cosmic wavelength region overlaps with more mundane terrestrial telecommunications.

In approaching redshifted 21-cm observations, although the first inkling might be to consider the mean emission signal in the bottom panel of Figure 14, the signal is orders of magnitude fainter than foreground synchrotron emission from relativistic electrons in the magnetic field of our own Milky Way as well as other galaxies (see Figure 17). Thus cosmologists have focused on the expected characteristic variations in T_b , both with position on the sky and especially with frequency, which signifies redshift for the cosmic signal. The synchrotron foreground is expected to have a smooth frequency spectrum, and so it is possible to isolate the cosmological signal by taking the difference in the sky brightness fluctuations at slightly different frequencies (as long as the frequency separation corresponds to the characteristic size of ionized bubbles). The 21-cm brightness temperature depends on the density of neutral hydrogen. As explained in the previous subsection, large-scale patterns in the reionization are driven by spatial variations in the abundance of galaxies; the 21-cm fluctuations reach ~ 5 mK (root mean square) in brightness temperature (Figure 15) on a scale of 10 Mpc (comoving). While detailed maps will be difficult to extract due to the foreground emission, a statistical detection of these fluctuations (through the power spectrum) is expected to be well within the capabilities of the first-generation experiments now being built. Current work suggests that the key information on the topology and timing of reionization can be extracted statistically.

Deleted:

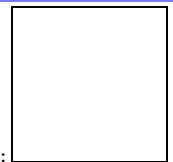


Figure 15. Close-up of cosmic evolution during the epoch of reionization, as revealed in a predicted 21-cm map of the IGM based on a numerical simulation (from Mellema et al. 2006). This map is constructed from slices of the simulated cubic box of side 150 Mpc (in comoving units), taken at

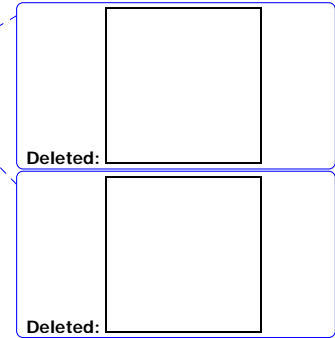
1 various times during reionization, which for the parameters of this particular simulation spans a
 2 period of 250 million years from redshift 15 down to 9.3. The vertical axis shows position χ in
 3 units of Mpc/h (where $h = 0.7$). This two-dimensional slice of the sky (one linear direction on the
 4 sky versus the line-of-sight or redshift direction) shows $\log_{10}(T_b)$, where T_b (in mK) is the 21-cm
 5 brightness temperature relative to the CMB. Since neutral regions correspond to strong emission
 6 (i.e., a high T_b), this slice illustrates the global progress of reionization and the substantial large-
 7 scale spatial fluctuations in reionization history. Observationally it corresponds to a narrow strip
 8 half a degree in length on the sky observed with radio telescopes over a wavelength range of 2.2 to
 9 3.4 m (with each wavelength corresponding to 21-cm emission at a specific redshift slice).

11 While numerical simulations of reionization are now reaching the cosmological box sizes needed to
 12 predict the large-scale topology of the ionized bubbles, they do this at the price of limited small-
 13 scale resolution (see Figure 16). These simulations cannot yet follow in any detail the formation of
 14 individual stars within galaxies, or the feedback that stars produce on the surrounding gas, such as
 15 photo-heating or the hydrodynamic and chemical impact of supernovae, which blow hot bubbles of
 16 gas enriched with the chemical products of stellar nucleosynthesis. Thus, the simulations cannot
 17 directly predict whether the stars that form during reionization are similar to the stars in the Milky
 18 Way and nearby galaxies or to the primordial $100M_{\odot}$ stars. They also cannot determine whether
 19 feedback prevents low-mass dark matter halos from forming stars. Thus, models are needed that
 20 make it possible to vary all these astrophysical parameters of the ionizing sources and to study the
 21 effect on the 21-cm observations.

23 Figure 16. Maps of the 21-cm brightness temperature comparing results of a numerical simulation
 24 and of two simpler numerical schemes, at three different redshifts (from Zahn et al. 2006). Each
 25 map is $65.6 \text{ Mpc}/h$ on a side, with a depth ($0.25 \text{ Mpc}/h$) that is comparable to the frequency
 26 resolution of planned experiments. The ionized fractions are $x_i = 0.13, 0.35$ and 0.55 for
 27 $z = 8.16, 7.26$ and 6.89 (top to bottom), respectively. All three maps show a very similar large-
 28 scale ionization topology. *Left column:* Numerical simulation, showing the ionized bubbles (black)
 29 produced by the ionizing sources (blue dots) that form in the simulation. *Middle column:* Numerical
 30 scheme that applies an analytical model to the final distribution of ionizing sources that form in the
 31 simulation. *Right column:* Numerical scheme that applies the analytical model to the linear density
 32 fluctuations that are the initial conditions of the simulation.

34 The theoretical expectations presented here for reionization and for the 21-cm signal are based on
 35 rather large extrapolations from observed galaxies to deduce the properties of much smaller
 36 galaxies that formed at an earlier cosmic epoch. Considerable surprises are thus possible, such as an
 37 early population of quasars or even unstable exotic particles that emitted ionizing radiation as they
 38 decayed. In any case, the forthcoming observational data in 21-cm cosmology should make the next
 39 few years a very exciting time.

41 At high redshifts prior to reionization, spatial perturbations in the thermodynamic gas properties are
 42 linear and can be predicted precisely (see section 1). Thus, if the gas is probed with the 21-cm
 43 technique then it becomes a promising tool of fundamental, precision cosmology, able to probe the
 44 primordial power spectrum of density fluctuations imprinted in the very early universe, perhaps in
 45 an era of cosmic inflation. The 21-cm fluctuations can be measured down to the smallest scales
 46 where the baryon pressure suppresses gas fluctuations, while the CMB anisotropies are damped on
 47 small scales (through the so-called Silk damping). This difference in damping scales can be seen by
 48 comparing the baryon-density and photon-temperature power spectra in Figure 4. Since the 21-cm
 49 technique is also three-dimensional (while the CMB yields a single sky map), there is a much large



1 potential number of independent modes probed by the 21-cm signal: $N_{21\text{-cm}} \sim 3 \times 10^{16}$ compared
 2 to $N_{\text{cmb}} \sim 2 \times 10^7$. This larger number should provide a measure of non-Gaussian deviations to a
 3 level of $\sim N_{21\text{cm}}^{-1/2}$, constituting a test of the inflationary origin of the primordial inhomogeneities
 4 which are expected to possess non-Gaussian deviations $> 10^{-6}$.

5
 6 The 21cm fluctuations are expected to simply trace the primordial power-spectrum of matter
 7 density perturbations (which is shaped by the initial conditions from inflation and the dark matter)
 8 either before the first population of galaxies had formed (at redshifts $z > 25$) or after reionization
 9 ($z < 6$) – when only dense pockets of self-shielded hydrogen (such as damped Ly α systems)
 10 survive. During the epoch of reionization, the fluctuations are mainly shaped by the topology of
 11 ionized regions, and thus depend on uncertain astrophysical details involving star formation.
 12 However, even during this epoch, the imprint of peculiar velocities (which are induced
 13 gravitationally by density fluctuations), can in principle be used to separate the implications for
 14 fundamental physics from the astrophysics.

15
 16 Figure 17. Predicted redshift evolution of the angle-averaged amplitude of the 21-cm power
 17 spectrum ($|\overline{\Delta T_b}| = [k^3 P_{21\text{-cm}}(k) / 2\pi^2]^{1/2}$) at comoving wavenumbers $k = 0.01$ (solid curve),
 18 0.1 (dotted curve), 1.0 (short dashed curve), 10.0 (long dashed curve), and 100.0 Mpc^{-1} (dot-
 19 dashed curve). In the model shown, reionization is completed at $z = 9.76$. The horizontal axis at
 20 the top shows the observed photon frequency at the different redshifts. The diagonal straight (red)
 21 lines show various factors of suppression for the synchrotron Galactic foreground, necessary to
 22 reveal the 21-cm signal (from Pritchard & Loeb 2008)
 23

24 Peculiar velocities imprint a particular form of anisotropy in the 21-cm fluctuations that is caused
 25 by gas motions along the line of sight. This anisotropy, expected in any measurement of density that
 26 is based on a spectral resonance or on redshift measurements, results from velocity compression.
 27 Consider a photon traveling along the line of sight that resonates with absorbing atoms at a
 28 particular point. In a uniform, expanding universe, the absorption optical depth encountered by this
 29 photon probes only a narrow strip of atoms, since the expansion of the universe makes all other
 30 atoms move with a relative velocity that takes them outside the narrow frequency width of the
 31 resonance line. If there is a density peak, however, near the resonating position, the increased
 32 gravity will reduce the expansion velocities around this point and bring more gas into the resonating
 33 velocity width. This effect is sensitive only to the line-of-sight component of the velocity gradient
 34 of the gas, and thus causes an observed anisotropy in the power spectrum even when all physical
 35 causes of the fluctuations are statistically isotropic. This anisotropy is particularly important in the
 36 case of 21-cm fluctuations. When all fluctuations are linear, the 21-cm power spectrum takes the
 37 form
 38

$$39 \quad P_{21\text{-cm}}(\mathbf{k}) = \mu^4 P_\rho(k) + 2\mu^2 P_{\rho\text{-iso}}(k) + P_{\text{iso}}, \quad (49)$$

40
 41 where $\mu = \cos\theta$ in terms of the angle θ between the wave-vector \mathbf{k} of a given Fourier mode and
 42 the line of sight, P_{iso} is the isotropic power spectrum that would result from all sources of 21-cm
 43 fluctuations without velocity compression, $P_\rho(k)$ is the 21-cm power spectrum from gas density
 44 fluctuations alone, and $P_{\rho\text{-iso}}(k)$ is the Fourier transform of the cross-correlation between the

1 density and all sources of 21-cm fluctuations. The three power spectra can also be denoted $P_{\mu^4}(k)$,
2 $P_{\mu^2}(k)$, and $P_{\mu^0}(k)$, according to the power of μ that multiplies each term. The prediction for
3 these power spectra at high redshift ($z > 20$), neglecting the effects of any stellar radiation, are
4 shown in Figure 18. At these redshifts, the 21-cm fluctuations probe the infall of the baryons into
5 the dark matter potential wells. The power spectrum shows remnants of the photon-baryon acoustic
6 oscillations on large scales, and of the baryon pressure suppression on small scales.

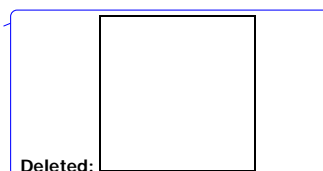
7
8 Figure 18. Power spectra of 21-cm brightness fluctuations versus comoving wavenumber (from
9 Barkana & Loeb 2005c). Show are the three power spectra that are separately observable, P_{μ^4}
10 (upper panel), P_{μ^2} (middle panel), and P_{μ^0} (lower panel). Each case shows redshifts 200, 150,
11 100, 50 (solid curves, from bottom to top), 35, 25, and 20 (dashed curves, from top to bottom).

12
13 Once stellar radiation becomes significant, many processes can contribute to the 21-cm fluctuations.
14 The contributions include fluctuations in gas density, temperature, ionized fraction, and Ly α flux.
15 These processes can be divided into two broad categories: The first, related to “*physics*”, consists
16 of probes of fundamental, precision cosmology, and the second, related to “*astrophysics*”, consists
17 of probes of stars. Both categories are interesting – the first for precision measures of cosmological
18 parameters and studies of processes in the early universe, and the second for studies of the
19 properties of the first galaxies. However, the astrophysics depends on complex non-linear processes
20 (collapse of dark matter halos, star formation, supernova feedback), and must be cleanly separated
21 from the physics contribution, in order to allow precision measurements of the latter. As long as all
22 the fluctuations are linear, the anisotropy noted above allows precisely this separation of the
23 *fundamental physics* from the *astrophysics* of the 21-cm fluctuations. In particular, the $P_{\mu^4}(k)$ is
24 independent of the effects of stellar radiation, and is a clean probe of the gas density fluctuations.
25 Once non-linear terms become important, there arises a significant mixing of the different terms; in
26 particular, this occurs on the scale of the ionizing bubbles during reionization.

27
28 The 21-cm fluctuations are affected by fluctuations in the Lyman- α flux from stars, a result that
29 yields an indirect method to detect and study the early population of galaxies at $z \sim 20$. The
30 fluctuations are caused by biased inhomogeneities in the density of galaxies, along with Poisson
31 fluctuations in the number of galaxies. Observing the power-spectra of these two sources would
32 probe the number density of the earliest galaxies and the typical mass of their host dark matter
33 halos. Furthermore, the enhanced amplitude of the 21-cm fluctuations from the era of
34 Ly α coupling improves considerably the practical prospects for their detection. Precise predictions
35 account for the detailed properties of all possible cascades of a hydrogen atom after it absorbs a
36 photon. Around the same time, X-rays may also start to heat the cosmic gas, producing strong 21-
37 cm fluctuations due to fluctuations in the X-ray flux.

38 39 4. Conclusions

40
41 The initial conditions of our Universe can be summarized on a single sheet of paper. Yet the
42 Universe is full of complex structures today, such as stars, galaxies and groups of galaxies. This
43 review discussed the standard theoretical model for how complexity emerged from the simple initial
44 state of the Universe through the action of gravity. In order to test and inform the related theoretical
45 calculations, large-aperture telescopes and arrays of radio antennae are currently being designed and
46 constructed.



1
2 The actual transition from simplicity to complexity has not been observed as of yet. The simple
3 initial conditions were already traced in maps of the microwave background radiation, but the
4 challenge of detecting the first generation of galaxies defines one of the exciting frontiers in the
5 future of cosmology. Once at hand, the missing images of the infant Universe might potentially
6 surprise us and revise our current ideas.

7 8 **Acknowledgements**

9
10 The author thanks his collaborators on the topics covered by this review: Dan Babich, Rennan
11 Barkana, Volker Bromm, Steve Furlanetto, Zoltan Haiman, Jonathan Pritchard, Stuart Wyithe, and
12 Matias Zaldarriaga.

13 14 **Glossary**

15
16 **Big Bang:** The point in time when the currently observed expansion of the Universe began.

17
18 **Hubble Parameter:** The ratio between the recession speed of distant cosmological sources and their distance, first
measured by Edwin Hubble.

19
20 **Cosmic Background Radiation:** The relic radiation left over from the hot and dense beginning of the Universe. The
21 Universe became nearly transparent to this radiation as soon as hydrogen formed out of free electrons and protons, 0.4
22 million years after the big bang. Prior to that time, scattering of the radiation on free electrons made the Universe
opaque.

23
24 **Baryons:** The family of sub-atomic particles which are made of three quarks, including the proton and the neutron
which make up atomic nuclei. This term is used in cosmology to denote ordinary (visible) matter.

25
26 **Dark Matter:** A hypothetical form of matter that does not interact with electromagnetic radiation, and whose presence
is inferred from its gravitational effects on visible matter.

27
28 **Redshift:** The stretching of a photon's wavelength by the cosmic expansion of space (resulting in the shift of optical
photons towards the red). The photon wavelength provides a yardstick that measures the so-called scale factor,

29 $a = (1 + z)^{-1}$, by which space was stretched between some early (emission) time to the present (observation) time.

30 By observing a series of known spectral lines from distant sources, it is possible to measure the source redshift from the
31 factor by which the wavelengths of these lines were increased relative to the values measured in the laboratory.

32 **Hydrogen:** The most abundant element in the Universe, which is made of an electron in a bound orbit around a proton.

33
34 **Ionization:** The freeing of an electron out of its bound orbit around a nucleus. Ionization can be caused by the
35 absorption of a photon (with energy greater than the binding energy of the electron), or as a result of an energetic
collision with another particle. Cosmic hydrogen was ionized during the early hot phase of the Universe, and then

36 formed abundantly at $z = 10^3$ when the cosmic temperature first dipped below a few thousand degrees K. The term
37 're-ionization' is used to denote the subsequent process by which cosmic hydrogen was ionized once again hundreds of
38 million of years later. Today most of the cosmic gas is ionized.

39
40 **Galaxies:** Condensations of matter in the Universe which make stars out of gas. The inner stellar core of galaxies is
often surrounded by a dark matter 'halo', whose presence is inferred through its gravitational effects.

41
42 **Power spectrum:** The square of the amplitude of the Fourier decomposition of the distribution of some quantity (such
43 as the matter density or the radiation brightness) in the Universe. The power spectrum, $P(\mathbf{k})$, is a function of the
wave_vector \mathbf{k} of the Fourier modes.

44
45 **Parsec:** A unit of length, equal to 3×10^{18} cm, abbreviated as 'pc'. A kilo-parsec (kpc) is a thousand pc, a mega-
46 parsec (Mpc) is a million pc, and a giga-parsec (Gpc) is a billion pc.

47 48 **Bibliography**

49
50 Abel T.L., Bryan G.L., Norman M.L. (2002). The Formation of the First Star in the Universe. *Science* 295 93. [Results
from simulations of the formation of the first stars].

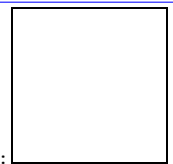
- 1 Allison A.C. and Dalgarno A. (1969). Spin Change in Collisions of Hydrogen Atoms. *Astrophys. J.* 158 423. [An early
2 paper about the effect of collisions on the spin temperature of hydrogen].
- 3 Arons J. and Wingert D.W. (1972). Theoretical Models of Photoionized Intergalactic Hydrogen. *Astrophys. J.* 177 1.
4 [An early discussion on the re-ionization of the intergalactic hydrogen, more than a quarter of a century before the topic
5 gained popularity].
- 6 Babich D. and Loeb A. (2006). Imprint of Inhomogeneous Reionization on the Power Spectrum of Galaxy Surveys at
7 High Redshifts. *Astrophys. J.* 640 1. [A discussion on the imprint of cosmic reionization on the distribution of low-mass
8 galaxies].
- 9 Barkana R. and Loeb A. (2001). In the beginning: the first sources of light and the reionization of the universe. *Phys.*
10 *Rep.* 349 125. [An overview on the physics of the first galaxies and reionization].
- 11 Barkana R. and Loeb A. (2004a). Gamma-Ray Bursts versus Quasars: Ly α Signatures of Reionization versus
12 Cosmological Infall. *Astrophys. J.* 601 64. [A comparison between quasars and gamma-ray bursts as probes of the
13 intergalactic medium at high redshifts].
- 14 Barkana R. and Loeb A. (2004b). Unusually Large Fluctuations in the Statistics of Galaxy Formation at High Redshift.
15 *Astrophys. J.* 609 474. [A discussion on the limitations of computer simulations of reionization owing to their finite size
16 of the simulated region].
- 17 Barkana R. and Loeb A. (2005a). A Method for Separating the Physics from the Astrophysics of High-Redshift 21
18 Centimeter Fluctuations. *Astrophys. J. Lett.* 624 L65. [The imprint of peculiar velocities on the 21cm brightness
19 fluctuations can be used to extract cosmological information during the epoch of reionization].
- 20 Barkana R. and Loeb A. (2005b). Detecting the Earliest Galaxies through Two New Sources of 21 Centimeter
21 Fluctuations. *Astrophys. J.* 626 1. [The imprint of the first galaxies on the 21cm fluctuations].
- 22 Barkana R. and Loeb A. (2005c). Probing the epoch of early baryonic infall through 21-cm fluctuations. *Mon. Not. Roy.*
23 *Astron. Soc. Lett.* 363 L36. [A discussion on the signature of acoustic oscillations on the 21cm brightness fluctuations].
- 24 Barkana R. and Loeb A. (2007). The physics and early history of the intergalactic medium. *Rep. Prog. Phys.* 70 627. [A
25 review on the history of the intergalactic medium].
- 26 Bennett C.L. et al. (1996). Four-Year COBE DMR Cosmic Microwave Background Observations: Maps and Basic
27 Results. *Astrophys. J. Lett.* 464 L1. [A description of the first robust detection of microwave background fluctuations by
28 the COBE satellite (for which the Nobel Prize was awarded in 2006)].
- 29 Bharadwaj S. and Ali S.S. (2004). The cosmic microwave background radiation fluctuations from HI perturbations prior
30 to reionization. *Mon. Not. Roy. Astron. Soc.* 352 142. [A discussion on the imprint of peculiar velocities on 21cm
31 fluctuations].
- 32 Bowman J.D., Morales M.F. and Hewitt J.N. (2006). The Sensitivity of First-Generation Epoch of Reionization
33 Observatories and Their Potential for Differentiating Theoretical Power Spectra. *Astrophys. J.* 638 20. [An early
34 discussion on the feasibility of modern measurements of the 21cm fluctuations from the epoch of reionization].
- 35 Bromm V., Coppi P.S., Larson R.B. (2002). The Formation of the First Stars. I. The Primordial Star-forming Cloud.
36 *Astrophys. J.* 564 23. [Results from numerical simulations of the formation of the first stars].
- 37 Bromm V. and Larson R.B. (2004). The First Stars. *Ann. Rev. Astron. & Astrophys.* 42 79. [An overview on the
38 formation of the first stars].
- 39 Bromm V. and Loeb A. (2003). Formation of the First Supermassive Black Holes. *Astrophys. J.* 596 34. [An early
40 model for the production of massive seeds for quasar black holes at early cosmic times].
- 41 Bromm V. and Loeb A. (2004). Accretion onto a primordial protostar. *New Astronomy* 9 353. [Results from high-
42 resolution simulations of the first stars, including an estimate of their final mass].
- 43 Bromm V., Kudritzki R.P. and Loeb A. (2001). Generic Spectrum and Ionization Efficiency of a Heavy Initial Mass
44 Function for the First Stars. *Astrophys. J.* 552 464. [A pioneering derivation of the spectrum of the first stars, and the
45 number of ionizing photons they produce per stellar mass].
- 46 Couchman, H.M.P. and Rees M.J. (1986). Pregalactic evolution in cosmologies with cold dark matter. *Mon. Not. Roy.*
47 *Astron. Soc.* 221 53. [A pioneering paper on the formation of the first galaxies in a CDM cosmology].
- 48 Chen X. and Miralda-Escudé J. (2004). The Spin-Kinetic Temperature Coupling and the Heating Rate due to Ly α
49 Scattering before Reionization: Predictions for 21 Centimeter Emission and Absorption. *Astrophys. J.* 602 1. [A detailed
50 calculation of the effect of Lyman- α photons on the spin temperature of intergalactic hydrogen].
- 51 Ciardi B., Ferrara A. and White S.D.M. (2003). Early reionization by the first galaxies. *Mon. Not. Roy. Astron. Soc.* 344
52 L7. [Results from simulations of reionization].

Deleted: prize

Deleted:

- 1 Ciardi B. and Loeb A. (2000). Expected Number and Flux Distribution of Gamma-Ray Burst Afterglows with High
2 Redshifts. *Astrophys. J.* 540 687. [An early calculation of the rate of gamma-ray bursts with high-redshifts].
- 3 Cole S. et al. (2005). The 2dF Galaxy Redshift Survey: power-spectrum analysis of the final data set and cosmological
4 implications. *Mon. Not. R. Astron. Soc.* 362 505. [Recent data on the distribution of galaxies on large spatial scales].
- 5 Dijkstra M., Haiman Z., Rees M.J. and Weinberg D.H. (2004). Photoionization Feedback in Low-Mass Galaxies at
6 High Redshift. *Astrophys. J.* 601 666. [A recent discussion on the suppression of low-mass galaxies after reionization].
- 7 Di Matteo T., Perna R., Abel T. and Rees M.J. (2002). Radio Foregrounds for the 21 Centimeter Tomography of the
8 Neutral Intergalactic Medium at High Redshifts. *Astrophys. J.* 564 576. [A discussion on the contaminating noise for
9 future 21cm observations].
- 10 Di Matteo T., Springel V., & Hernquist, L. (2005). Energy input from quasars regulates the growth and activity of black
11 holes and their host galaxies. *Nature*, 433, 604. [Simulations of quasar feedback on galaxy formation and evolution].
- 12 Eisenstein D.J. et al. (2005). Detection of the Baryon Acoustic Peak in the Large-Scale Correlation Function of SDSS
13 Luminous Red Galaxies. *Astrophys. J.* 633 560. [The first detection of baryonic oscillations in the distribution of
14 galaxies].
- 15 Efstathiou G. (1992). Suppressing the formation of dwarf galaxies via photoionization. *Mon. Not. Roy Astron. Soc.* 256
16 43. [An early discussion on the suppression of dwarf galaxies by ionizing radiation].
- 17 Ellis R. (2008). Observations of the High Redshift Universe. *SAAS-Fee Advanced Course 36*, Springer Verlag, Berlin
18 2008. <http://arxiv.org/abs/astro-ph/0701024>. [A recent overview of the status of observations of high-redshift galaxies].
- 19 Fan X. et al. (2002). Evolution of the Ionizing Background and the Epoch of Reionization from the Spectra of $z \sim 6$
20 Quasars. *Astron. J.* 123 1247. [Observational constraints on intergalactic hydrogen from the spectra of quasars which
21 formed a billion years after the big bang].
- 22 Fan X. et al. (2003). A Survey of $z > 5.7$ Quasars in the Sloan Digital Sky Survey. II. Discovery of Three Additional
23 Quasars at $z > 6$. *Astron. J.* 125 1649. [Observations of high redshift quasars].
- 24 Fan X. et al. (2005). Constraining the Evolution of the Ionizing Background and the Epoch of Reionization with
25 $z \sim 6$ Quasars II: A Sample of 19 Quasars. *Astron. J.* 132 (2006) 117. [A description of the sample of the highest-
26 redshift quasars].
- 27 Fan X., Carilli C.L. and Keating B. (2006). Observational Constraints on Cosmic Reionization. *Ann. Rev. Astron. &*
28 *Astrophys.* 44 415. [A review on the constraints drawn from quasar spectra about reionization].
- 29 Field G.B. (1958). Excitation of the Hydrogen 21 cm Line. *Proc. IRE* 46 240. [A classic paper on the physics of the 21
30 cm line of intergalactic hydrogen].
- 31 Field G.B. (1959). The Time Relaxation of a Resonance-Line Profile. *Astrophys. J.* 129 551. [A pioneering paper on the
32 physics of the 21 cm line from intergalactic hydrogen].
- 33 Fukugita M. and Kawasaki M. (1994). Reionization during Hierarchical Clustering in a Universe Dominated by Cold
34 Dark Matter. *Mon. Not. Roy. Astron. Soc.* 269 563. [An early discussion on cosmic reionization, about a decade before
35 the topic gained popularity].
- 36 Furlanetto S.R. and Loeb A. (2003). Metal Absorption Lines as Probes of the Intergalactic Medium Prior to the
37 Reionization Epoch. *Astrophys. J.* 588 18. [A discussion on the detectability of absorption lines from heavy elements
38 which were produced in stellar interiors and then dispersed into intergalactic space].
- 39 Furlanetto S.R., Zaldarriaga M. and Hernquist L. (2004). The Growth of H II Regions During Reionization. *Astrophys.*
40 *J.* 613 1. [A calculation of the size distribution of ionized bubbles during the epoch of reionization].
- 41 Furlanetto S.R., Oh S.P. and Briggs F. (2006). Cosmology at low frequencies: The 21 cm transition and the high-
42 redshift Universe. *Phys. Rep.* 433 181. [An overview on 21cm cosmology].
- 43 Gehrels N. et al. (2004). The Swift Gamma-Ray Burst Mission. *Astrophys. J.* 611 1005. [A description of the SWIFT
44 satellite that is currently detecting gamma-ray bursts and their afterglows].
- 45 Gnedin N.Y. and Ostriker J.P. (1997). Reionization of the Universe and the Early Production of Metals. *Astrophys. J.*
46 486 581. [An early numerical simulation of the production of heavy elements during the epoch of reionization].
- 47 Gnedin N.Y. and Hui L. (1998). Probing the Universe with the Lyman-alpha forest - I. Hydrodynamics of the low-
48 density intergalactic medium. *Mon. Not. Roy Astron. Soc.* 296 44. [A simple model for the Lyman- α forest in quasar
49 spectra].
- 50 Gnedin N.Y. (2000). Effect of Reionization on Structure Formation in the Universe. *Astrophys. J.* 542 535. [Results

Deleted:



1 from early simulations of the effect of reionization on the assembly of gas into low-mass galaxies].

2 Goodman J. (1995). Geocentrism reexamined. *Phys. Rev. D* 52 1821. [A discussion on existing evidence for the
3 homogeneity of the Universe].

4 Gunn J.E. and Peterson B.A. (1965). On the Density of Neutral Hydrogen in Intergalactic Space. *Astrophys. J.* 142
5 1633. [A seminal paper on the Lyman- α absorption feature of intergalactic hydrogen].

6 Haiman Z., Thoul A.A. and Loeb A. (1996). Cosmological Formation of Low-Mass Objects. *Astrophys. J.* 464 52. [The
7 first (spherically-symmetric) simulation of the formation of the first gas-rich galaxies].

8 Haiman Z. and Loeb A. (1997). Signatures of Stellar Reionization of the Universe. *Astrophys. J.* 483 21. [An early
9 detailed calculation of reionization by stars in the modern context of cosmological structure formation].

10 Haiman Z., Rees M.J., Loeb A. (1997). Destruction of Molecular Hydrogen during Cosmological Reionization.
11 *Astrophys. J.* 476 458; erratum – *Astrophys. J.* 484 985. [Negative feedback of UV photons on the production of
12 molecular hydrogen in the first galaxies].

13 Haislip J. et al. (2006). A photometric redshift of $z = 6.39 \pm 0.12$ for GRB 050904. *Nature* 440 181. [The
14 discovery of a gamma-ray burst with the highest redshift known].

15 Hirata C.M. (2006). Wouthuysen-Field coupling strength and application to high-redshift 21-cm radiation. *Mon. Not.
16 Roy. Astron. Soc.* 367 259. [A detailed discussion on the coupling between the spin temperature and the kinetic
17 temperature of hydrogen through its interaction with Lyman- α photons].

18 Hogan C.J. and Rees M.J. (1979). Spectral appearance of non-uniform gas at high Z . *Mon. Not. Roy. Astron. Soc.* 188
19 791. [A pioneering discussion on the use of resonant lines to probe the intergalactic gas and study cosmology].

20 Hu E.M., Cowie L.L., McMahon R.G., Capak P., Iwamuro F., Kneib J.P., Maihara T. and Motohara K. (2002). A
21 Redshift $z=6.56$ Galaxy behind the Cluster Abell 370. *Astrophys. J. Lett.* 568 L75. [A spectroscopic detection of one of
22 the earliest galaxies known].

23 Iye M. et al. (2006). A galaxy at a redshift $z = 6.96$. *Nature* 443 186. [A spectroscopic detection of one of the earliest
24 galaxies known].

25 Kaiser N. (1984). On the spatial correlations of Abell clusters. *Astrophys. J. Lett.* 284 L9. [A pioneering discussion on
26 the concept of bias in the clustering statistics of cosmological objects].

27 Kaiser N. (1987). Clustering in real space and in redshift space. *Mon. Not. Roy. Astron. Soc.* 227 1. [A pioneering
28 discussion on the effect of peculiar velocities on the clustering of sources in redshift surveys].

29 Kamionkowski M., Spergel D.N. and Sugiyama N. (1994). Small-scale cosmic microwave background anisotropies as
30 probe of the geometry of the universe. *Astrophys. J. Lett.* 426 L57. [An early discussion on the use of microwave
31 background data to constrain the underlying geometry of the Universe].

32 Kitayama T. and Ikeuchi S. (2000). Formation of Subgalactic Clouds under Ultraviolet Background Radiation.
33 *Astrophys. J.* 529 615. [Spherically-symmetric simulations of the suppressing effect of UV radiation on the collapse
34 low-mass gas clouds].

35 Kolb E.W. and Turner M.S. (1990). The early universe. (Redwood City, CA: Addison-Wesley). [A textbook on the
36 interface between modern cosmology and particle physics].

37 Komatsu E. et al. (2008). Five-Year Wilkinson Microwave Anisotropy Probe (WMAP) Observations: Cosmological
38 Interpretation, ArXiv e-prints, 803, arXiv:0803.0547. [The latest cosmological constraints based on five-years of data
39 gathering by the WMAP satellite].

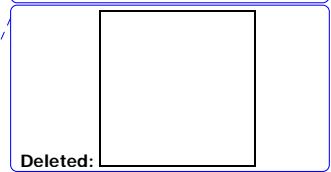
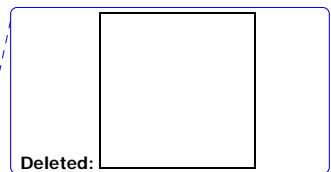
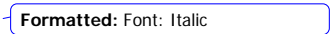
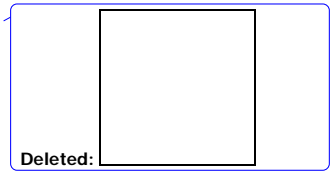
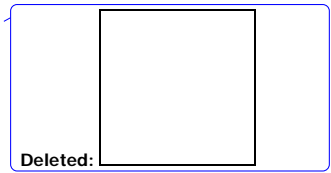
40 Lamb D.Q and Reichart D.E. (2000). Gamma-Ray Bursts as a Probe of the Very High Redshift Universe. *Astrophys. J.*
41 536 1. [An early discussion on the detectability of gamma-ray bursts out to very high redshifts].

42 Lidz A., Oh S.P. and Furlanetto S.R. (2006). Have We Detected Patchy Reionization in Quasar Spectra? *Astrophys. J.*
43 *Lett.* 639 L47. [An analysis of the implications from absorption spectra of high-redshift quasar for models of
44 reionization].

45 Loeb A. (2008). First Light. *SAAS-Fee Advanced Course 36*, Springer Verlag, Berlin 2008. <http://arxiv.org/abs/astro-ph/0701024>. [A recent overview of the underlying physics in studies of the first galaxies].

47 Loeb A. (2006). The dark ages of the Universe. *Scientific American*, 295, 46
48 (<http://www.cfa.harvard.edu/loeb/sciam.pdf>). [A popular level review on the first galaxies and 21-cm cosmology].

49 Loeb A. and Rybicki G. (1999). Scattered Lyman- α Radiation around Sources before Cosmological Reionization
50 *Astrophys. J.* 524, 527. [A derivation of the halo of scattered Lyman- α photons around a source embedded in an



1 expanding intergalactic medium].

2 Loeb A. and Zaldarriaga M. (2004). Measuring the Small-Scale Power Spectrum of Cosmic Density Fluctuations
3 through 21cm Tomography Prior to the Epoch of Structure Formation. *Phys. Rev. Lett.* 92 211301. [The first calculation
4 of the power-spectrum of 21-cm brightness fluctuations during the dark ages [prior to the appearance of the first
5 galaxies]].

6 Loeb A. and Wyithe S. (2008). Precise Measurement of the Cosmological Power Spectrum With a Dedicated 21cm
7 Survey After Reionization. *Phys. Rev. Lett.* in press, ArXiv e-prints, 801, arXiv:0801.1677. [A study demonstrating that
8 future 21cm data after reionization can map the matter distribution through most of the observable volume of the
9 Universe].

10 Ma C. and Bertschinger E. (1995). Cosmological Perturbation Theory in the Synchronous and Conformal Newtonian
11 Gauges. *Astrophys. J.* 455 7. [A comprehensive discussion on the growth of structure in the Universe].

12 Madau P., Meiksin A. and Rees M.J. (1997). 21 Centimeter Tomography of the Intergalactic Medium at High Redshift.
13 *Astrophys. J.* 475 429. [An early discussion on the use of the 21 cm line for three-dimensional mapping of intergalactic
14 hydrogen].

15 McQuinn M., Zahn O., Zaldarriaga M., Hernquist L. and Furlanetto S.R. (2006). Cosmological Parameter Estimation
16 Using 21 cm Radiation from the Epoch of Reionization. *Astrophys. J.* 653 815. [A demonstration of the power of
17 statistical analysis of future 21 cm data for constraining cosmological parameters].

18 Mellema G., Iliiev I.T., Pen U.L. and Shapiro P.R. (2006). Simulating Cosmic Reionization at Large Scales II: the 21-
19 cm Emission Features and Statistical Signals. *Mon. Not. Roy. Astron. Soc.* 372 679. [Results from a numerical
20 simulation of reionization by the first galaxies].

21 Miralda-Escudé J. (1998). Reionization of the Intergalactic Medium and the Damping Wing of the Gunn-Peterson
22 Trough. *Astrophys. J.* 501 15. [A derivation of the spectral profile of Lyman- α absorption by a neutral intergalactic
23 medium around a high-redshift source].

24 Miralda-Escudé J. and Rees M J (1998). Searching for the Earliest Galaxies Using the Gunn-Peterson Trough and the
25 Lyman-alpha Emission Line. *Astrophys. J.* 497 21. [An early discussion on the spectral signatures of high-redshift
26 galaxies].

27 Miralda-Escudé J. (2000). Soft X-Ray Absorption by High-Redshift Intergalactic Helium. *Astrophys. J. Lett.* 528 L1. [A
28 discussion on the absorption signature of a neutral intergalactic medium around an X-ray source].

29 Murray N., Quataert E. and Thompson T.A. (2005). On the Maximum Luminosity of Galaxies and Their Central Black
30 Holes: Feedback from Momentum-driven Winds. *Astrophys. J.* 618 569. [A model for momentum-regulated growth of
31 supermassive black holes in galaxies].

32 Naoz S. and Barkana R. (2005). Growth of linear perturbations before the era of the first galaxies. *Mon. Not. Roy.*
33 *Astron. Soc.* 362 1047. [A precise calculation of the linear evolution of density and temperature fluctuations in the
34 cosmic gas during the dark ages].

35 Navarro J. F., Frenk C. S., White S. D. M. (1997). A Universal Density Profile from Hierarchical Clustering.
36 *Astrophysical Journal* 490, 493. [Results from numerical simulations that demonstrated the existence of a universal
37 form for the density profile in dark matter halos].

38 Navarro J.F. and Steinmetz M. (1997). The Effects of a Photoionizing Ultraviolet Background on the Formation of Disk
39 Galaxies. *Astrophys. J.* 478 13. [Results from three-dimensional simulations on the effect of UV radiation on the
40 assembly of gas in low-mass galaxies].

41 Oh S. P. (2001). Reionization By Hard Photons. I. X-Rays From the First Star Clusters. *Astrophys. J.* 553 499. [A
42 discussion on reionization by X-ray photons].

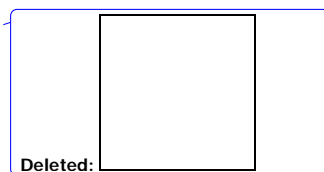
43 Osterbrock D.E. (1974). Astrophysics of gaseous nebulae. (San Francisco: W. H. Freeman and Company) p.14. [A
44 textbook describing the physics of ionized regions around a UV source].

45 Peebles P.J.E. (1980). The large-scale structure of the universe. (Princeton: Princeton University Press). [A textbook
46 describing basic concepts related to the growth of structure in the Universe].

47 Peebles P.J.E. (1984). Dark matter and the origin of galaxies and globular star clusters. *Astrophys. J.* 277 470. [A
48 pioneering discussion on cold dark matter in galaxies].

49 Peebles P.J.E. (1993). Principles of physical cosmology. (Princeton: Princeton University Press). [A textbook on basic
50 concepts in the physics of cosmology].

51 Peebles P.J.E. and Yu J.T. (1970). Primeval Adiabatic Perturbation in an Expanding Universe. *Astrophys. J.* 162 815.
52 [A pioneering calculation of the temperature anisotropies of the microwave background].



1 Pritchard J.R. and Furlanetto S.R. (2006) Descending from on high: Lyman-series cascades and spin-kinetic
2 temperature coupling in the 21-cm line. *Mon. Not. Roy. Astron. Soc.* 367 1057. [A comprehensive discussion on the
3 effect of Lyman-series photons on the spin temperature of hydrogen and the corresponding 21-cm fluctuations].

4 Pritchard J.R. and Furlanetto S.R. (2007). 21 cm fluctuations from inhomogeneous X-ray heating before reionization.
5 *Mon. Not. Roy. Astron. Soc.* 376 1680. [A study of the effect of inhomogeneous X-ray heating by the first galaxies on
6 21-cm fluctuations].

7 Pritchard J.R. and Loeb A. (2008). Evolution of the 21 cm signal throughout cosmic history. ArXiv e-prints, 802,
8 arXiv:0802.2102. [A comprehensive summary of the various sources of 21-cm fluctuations at all redshifts].

9 Purcell E.M. and Field G.B. (1956). Influence of Collisions upon Population of Hyperfine States in Hydrogen.
10 *Astrophys. J.* 124 542. [A pioneering paper on the effect of atomic collisions on the spin temperature of hydrogen].

11 Quinn T., Katz N. and Efstathiou G. (1996). Photoionization and the formation of dwarf galaxies. *Mon. Not. Roy*
12 *Astron. Soc. Lett.* 278 49. [Results from simulations concerning the suppressing effect of ionizing radiation on the
13 assembly of gas in low-mass galaxies].

14 Rees M.J. and Sciama D.W. (1968). Larger scale Density Inhomogeneities in the Universe. *Nature* 217 511. [A
15 pioneering discussion on the imprint of large scale inhomogeneities on temperature anisotropies of the microwave
16 background through the time-dependence of the gravitational potential].

17 Sachs R.K. and Wolfe A.M. (1967). Perturbations of a Cosmological Model and Angular Variations of the Microwave
18 Background. *Astrophys. J.* 147 73. [A pioneering formal derivation of the temperature anisotropies in the microwave
19 background owing to density fluctuations].

20 Scott D. and Rees M.J. (1990). The 21-cm line at high redshift: a diagnostic for the origin of large scale structure. *Mon.*
21 *Not. Roy. Astron. Soc.* 247 510. [An early discussion on the potential use of the 21-cm line for cosmological studies].

22 Seljak U. and Zaldarriaga M. (1996). A Line-of-Sight Integration Approach to Cosmic Microwave Background
23 Anisotropies. *Astrophys. J.* 469 437. [An efficient simplified solution to the equations that provide the microwave
24 background anisotropies].

25 Shapiro P.R. and Giroux M.L. (1987). Cosmological H II regions and the photoionization of the intergalactic medium.
26 *Astrophys. J. Lett.* 321 L107. [An early discussion on the evolution of ionized regions around a UV source embedded
27 within an expanding medium of cosmic gas].

28 Shapiro P.R., Giroux M.L. and Babul A. (1994). Reionization in a cold dark matter universe: The feedback of galaxy
29 formation on the intergalactic medium. *Astrophys. J.* 427 25. [An early discussion on reionization by galaxies].

30 Silk J. (1968). Cosmic Black-Body Radiation and Galaxy Formation. *Astrophys. J.* 151 459. [A pioneering derivation of
31 the effect of photon diffusion on the damping of microwave background anisotropies on small scales].

32 Silk J. and Rees M.J. (1998). Quasars and Galaxy Formation. *Astron. & Astrophys.* 331 L1. [A schematic discussion on
33 the expected scaling relations between central black hole mass and velocity dispersion in galaxies, based on self-
34 regulated growth by momentum or energy feedback].

35 Stark D.P., Loeb A. and Ellis R. (2007). An Empirically Calibrated Model for Interpreting the Evolution of Galaxies
36 during the Reionization Era. *Astrophys. J.* 668 627. [A simple theoretical model for observations of high redshift
37 galaxies].

38 Sunyaev R.A. and Zeldovich Y.B. (1970). Small-Scale Fluctuations of Relic Radiation. *APSS* 7 3. [A pioneering
39 derivation of the acoustic oscillation signature in the anisotropies of the microwave background].

40 Tegmark M. et al. (1997). How Small Were the First Cosmological Objects? *Astrophys. J.* 474 1. [An early discussion
41 on the conditions for the formation of the first galaxies].

42 Thoul A.A. and Weinberg D.H. (1996). Hydrodynamic Simulations of Galaxy Formation. II. Photoionization and the
43 Formation of Low-Mass Galaxies. *Astrophys. J.* 465 608. [Results from a spherically-symmetric simulation of the
44 suppressed collapse of gas clouds under the influence of a UV radiation background].

45 Totani T., Kawai N., Kosugi G., Aoki K., Yamada T., Iye M., Ohta K. and Hattori T. (2006). Implications for Cosmic
46 Reionization from the Optical Afterglow Spectrum of the Gamma-Ray Burst 050904 at $z = 6.3$. *Pub. Astron. Soc.*
47 *Japan* 58 485. [A discussion on the implication from the spectral data of the gamma-ray burst with the highest known
48 redshift].

49 Trac H., and Cen R. (2007). Radiative Transfer Simulations of Cosmic Reionization. I. Methodology and Initial Results.
50 *Astrophys. J.* 671 1. [Results from a state-of-the-art computer simulation of cosmic reionization].

51 Verner D.A., Ferland G.J., Korista T. and Yakovlev D.G. (1996). Atomic Data for Astrophysics. II. New Analytic FITS
52 for Photoionization Cross Sections of Atoms and Ions. *Astrophys. J.* 465 487. [A compilation of photo-ionization cross

1 sections for a variety of atomic and ionic species].

2 Weinberg S. (1972). *Gravitation and Cosmology: Principles and Applications of the General Theory of Relativity.*

3 *Gravitation and Cosmology* (New York: Wiley). [A pioneering textbook that established the currently popular link

4 between cosmology and particle physics].

5 Weinberg D.H., Hernquist L. and Katz N. (1997). Photoionization, Numerical Resolution, and Galaxy Formation.

6 *Astrophys. J.* 477 8. [Results from numerical simulations on the effect of ionizing radiation on galaxy formation].

7 White R.L., Becker R.H., Fan X., Strauss M.A. (2003). Probing the Ionization State of the Universe at $z > 6$. *Astron.*

8 *J.* 126 1. [A study of the inference from quasar spectra concerning the ionization state of the intergalactic medium at

9 redshift $z > 6$].

10 Wouthuysen S.A. (1952). On the excitation mechanism of the 21-cm (radio-frequency) interstellar hydrogen emission

11 line. *Astron. J.* 57 31. [A pioneering study of the effect of Lyman- α photons in coupling the spin temperature of

12 hydrogen to its kinetic temperature].

13 Wu K.K.S., Lahav O. and Rees M.J. (1999). The large-scale smoothness of the Universe. *Nature* 397 225. [A summary

14 of the evidence for the isotropy and homogeneity of the Universe].

15 Wyithe J.S.B. and Loeb A. (2003). Self-regulated Growth of Supermassive Black Holes in Galaxies. *Astrophys. J.* 595

16 614. [An early model for self-regulated growth of quasars and their resulting luminosity function].

17 Wyithe J.S.B. and Loeb A. (2004a). A large neutral fraction of cosmic hydrogen a billion years after the Big Bang.

18 *Nature* 427 815. [A study linking the size of the ionized regions around high-redshift quasars with the neutral fraction

19 of the intergalactic medium].

20 Wyithe J.S.B. and Loeb A. (2004b). A characteristic size of ~ 10 Mpc for the ionized bubbles at the end of cosmic

21 reionization. *Nature* 432 194. [A model-independent derivation of the characteristic size of ionized bubbles at the end of

22 the reionization epoch].

23 Wyithe J.S.B., Loeb A. and Barnes D.G. (2005). Prospects for Redshifted 21 cm Observations of Quasar H II Regions.

24 *Astrophys. J.* 634 715. [A study of the feasibility of detecting ionized regions around high-redshift quasars as cavities in

25 21-cm surveys].

26 Wyithe J.S.B., and Loeb A. (2008). Fluctuations in 21-cm emission after reionization. *Mon. Not. Roy. Astron. Soc.*, 383,

27 606. [A derivation of 21-cm fluctuations at low redshifts owing to dense (Galactic) pockets of hydrogen that are self-

28 shielded from the UV background after reionization].

29 Wyithe J.S.B., Loeb A. and Geil P.M. (2008). Baryonic acoustic oscillations in 21-cm emission: a probe of dark energy

30 out to high redshifts. *Mon. Not. Roy. Astron. Soc.* 383, 1195. [A study of the detectability of baryonic acoustic

31 oscillations in the 21-cm brightness fluctuations after reionization].

32 Yamamoto K., Sugiyama N. and Sato H. (1997). Cosmological baryon sound waves coupled with the primeval

33 radiation. *Phys. Rev. D* 56 7566. [A comprehensive discussion on the underlying physics of acoustic oscillations].

34 Yoshida N., Omukai K., Hernquist L., and Abel T. (2006). Formation of Primordial Stars in a LCDM Universe.

35 *Astrophys. J.* 652 6. [Simulations of the formation of the first stars over a large cosmological region].

36 Zahn O., Lidz A., McQuinn M., Dutta S., Hernquist L., Zaldarriaga M. and Furlanetto S.R. (2006). Simulations and

37 Analytic Calculations of Bubble Growth During Hydrogen Reionization. *Astrophys. J.* 654 12. [Results from

38 simulations of the evolution of cosmic reionization].

39 Zhang W., Woosley S. and MacFadyen A.I. (2003). Relativistic Jets in Collapsars. *Astrophys. J.* 586 356. [Simulations

40 of the popular collapsar model for long-duration gamma-ray bursts, in which relativistic jets are produced by the

41 collapse of a stellar core to a black hole].

42 Zygelman B. (2005). Hyperfine Level-changing Collisions of Hydrogen Atoms and Tomography of the Dark Age

43 Universe. *Astrophys. J.* 622 1356. [A detailed discussion on the effect of atomic collisions on the spin temperature of

44 cosmic hydrogen].

45 46 **Biographical Sketch**

47
48 **Abraham (Avi) Loeb** is a theoretical physicist working on astrophysics and cosmology. He is currently a professor of

49 astronomy and the director of the Institute for Theory and Computation (ITC) at Harvard University. Loeb was born in

50 Israel in 1962 and took part in the national Talpiot program before receiving a BSc, MSc, and PhD degrees (in Plasma

51 Physics) at age 24 from the Hebrew University in Jerusalem.

52 Between 1988-1993, he was long-term member at the Institute for Advanced Study in Princeton, where he started to

1 work in theoretical astrophysics. In 1993 he moved to Harvard University as an assistant professor in the department of
2 astronomy, where he was tenured three years later. He was given a number of awards including the Guggenheim
3 Fellowship in 2002. He also holds a visiting professorship at the Weizmann Institute of Science. He is broadly regarded
4 as an authority on studies of the first stars and of supermassive black holes in galaxies. His published work includes
5 nearly 300 papers in refereed journals, as well as a book and a patent.
6 Prof. Loeb has worked on broad range of research areas in astrophysics and cosmology, including the first stars, the
7 epoch of reionization, the formation and evolution of massive black holes, gravitational lensing, gamma-ray bursts, and
8 21-cm cosmology. Some of his papers are considered as pioneering in areas that have become by now the focus of
9 established communities of astrophysicists. In particular, Loeb was among the first theorists to trigger the current
10 research on the first stars and quasars. In a series of papers with his students and postdocs, he addressed how and when
11 the first stars and black holes formed and what effects they had on the young universe. In 2006 Prof. Loeb was featured
12 in a cover story of TIME magazine on the first stars and in a Scientific American article on the dark ages of the
13 Universe. In 2008 Prof. Loeb was featured in a cover story of Smithsonian magazine on black holes and in a cover story
14 of Astronomy magazine on the future collision between the Milky-Way and Andromeda.